

Contents lists available at ScienceDirect

Automatica

journal homepage: www.elsevier.com/locate/automatica



Data-driven robust iterative learning control of linear systems[★]

Zezhou Zhang, Qingze Zou*

Rutgers, State University of New Jersey, Piscataway, NJ, 08854, USA



ARTICLE INFO

Article history:
Received 21 February 2023
Received in revised form 7 December 2023
Accepted 16 February 2024
Available online xxxx

Keywords: Data-driven Iterative learning control Multi-input multi-output systems Precision output tracking

ABSTRACT

We propose a data-driven robust iterative learning control (ILC) technique to multi-input-multi-output (MIMO) linear systems. Control of MIMO linear systems, particularly with strong cross-axis coupling, is challenging as modeling of a MIMO system can be complicated, time-consuming, and often requires a trade-off between robustness and performance. As such, limitations exist in current ILC techniques. The aim of this paper is to develop an efficient and easy-to-use data-driven ILC technique to output tracking of MIMO linear systems under random disturbance. Through the proposed technique, the complicated modeling process and the robustness-accuracy trade-off are avoided, and the up-to-now system dynamics is captured by constructing and updating the iteration gain using the input and output data in the last iteration. It is shown that monotonic convergence of the ILC algorithm is guaranteed, and an optimal gain can be obtained to maximize the convergence rate and minimize the residual tracking error. The proposed technique is illustrated through experiments on a three-input three-output piezoelectric actuator system, with comparison to the adaptive multi-axis inversion-based iterative control (A-MAIIC) technique. The experimental results show rapid convergence and improved formance of the proposed technique when the cross-axis coupling is strong.

© 2024 The Author(s). Published by Elsevier Ltd. This is an open access article under the CC BY-NC license (http://creativecommons.org/licenses/by-nc/4.0/).

1. Introduction

A data-driven iterative learning control (DD-ILC) technique is proposed for output tracking of multi-input multi-output (MIMO) systems under random output disturbance. Precision tracking of MIMO systems is needed in various applications, ranging from advanced manufacturing (Armstrong & Alleyne, 2021), atomic force microscope (AFM) (Yan, Wang, & Zou, 2012), robot manipulation (Yan et al., 2021) to semiconductor fabrication (Dirkx, van de Wijdeven, & Oomen, 2020). In these applications, iterative learning control (ILC) becomes a natural choice due to the periodic motion involved (Chen & Tomizuka, 2013). However, existing ILC techniques face challenges in modeling, trade-off between performance and robustness, and system dynamics complexity. This motivates the development of a DD-ILC approach in this work.

Limitations exist in current ILC techniques to achieve highspeed precision tracking of MIMO systems. For model-based ILC techniques (Bristow, Tharayil, & Alleyne, 2006), modeling of a

E-mail addresses: zezhou.zhang@rutgers.edu (Z. Zhang), qzzou@soe.rutgers.edu (Q. Zou).

MIMO system can be time-consuming and complicated, particularly when the dimension of the system increases. For example, both the structure and the order of the model need to be determined, and the model quality can be sensitive to the measurement noise and the unmodeled dynamics. The complexity of the modeling process can be alleviated by only modeling the diagonal dynamics of the system (Yan et al., 2012). Through a frequencydomain inversion-based framework, efficient and precision output tracking can be achieved (Yan et al., 2012). However, this simplification requires the diagonal dynamics to be dominant over the cross axis ones, i.e., the cross-axis coupling dynamics is relatively weak. Alternatively, a constant proportional-integralderivative (PID) type of ILC algorithm (Hao, Zhang, & Li, 2008) has been proposed that avoids modeling the system dynamics. This relatively simple ILC method, however, is slow in convergence (e.g., over 200 iterations in Hao et al., 2008) and the working bandwidth is low, resulting in poor performance as the speed of the desired trajectory increases towards the resonant frequency of the system. Although the working bandwidth can be increased by using system dynamics model to optimize the ILC controller (Mandra, Galkowski, Rauh, Aschemann, & Rogers, 2020), the design of the robustness filter becomes complicated when the order of the system increases—when the cross-axis coupling becomes strong and the number of inputs/outputs increases, as the robustness filter for each input-output channel needs to be individually designed. Therefore, further development of ILC is needed to simplify or even avoid the modeling process, without

This work was supported by NSF CMMI-1851907, IIBR-1952823, and PFI-2234449. The material in this paper was partially presented at the 2023 American Control Conference (ACC), May 31–June 2, 2023, San Diego, California, USA. This paper was recommended for publication in revised form by Associate Editor Andrea Cristofaro under the direction of Editor Sophie Tarbouriech.

^{*} Corresponding author.

loss of efficiency in convergence and efficacy in high-speed tracking, even in the presence of strong cross-coupling dynamics and external disturbance.

Recent development in DD-ILC provides an effective avenue to address these issues in modeling and cross-coupling dynamics. The input-output data acquired in past iterations are directly used to construct the system dynamics model and update the control input. As such, no additional modeling process is needed, and as changes of the system dynamics are directly reflected and captured in the past input-output data, both performance and robustness of the ILC technique are improved. For example, the Hessian information has been explored in a DD-ILC technique to increase the convergence rate (Bolder, Kleinendorst, & Oomen, 2018). The design of the weight matrices, however, requires a priori expertise knowledge gained from a large number of experiments. This requirement can be mitigated by estimating the linearized system dynamics through extra iterations (Yu, Hou, Polycarpou, & Duan, 2020). The number of experiments needed has also been reduced through a stochastic-based DD-ILC approach (Aarnoudse & Oomen, 2020). However, only is the convergence of the expectation of the tracking error considered the variation is not characterized, and the iteration coefficients need to be carefully tuned, resulting in conservative performance and slow convergence (Aarnoudse & Oomen, 2020). The technique has been further enhanced to improve the tracking performance (Wang & Zou, 2023), where the input-output data in a differential format is used to design the learning filter, and it is shown that both the linear dynamics and the hysteresis can be accounted for simultaneously (Wang & Zou, 2023). However, the algorithm is limited to SISO systems only. Therefore, how to achieve both rapid convergence and robust performance for MIMO systems with strong cross-axis coupling remains as challenging for DD-ILC.

The main contribution of this paper is the development of a DDRO-ILC method for MIMO systems. Specifically, tracking of trajectories with a finite discrete spectrum is considered, and the input-output data obtained in past iterations are formatted as "snapshot" (Brunton & Kutz, 2022) in frequency domain, and then used to approximate the system inverse in the iteration gain via the singular value decomposition (SVD) technique. A fast SVD (fSVD) algorithm is proposed to accelerate the computation. Moreover, an optimal gain is designed to maximize the convergence rate and minimize the tracking error against random disturbance. Partial preliminary results of this work have been presented recently in conference (Zhang & Zou, 2023). We substantially enrich the theoretical results through a rigorous development of input initialization, convergence analysis, and iterative gain optimization, and an algorithm to accelerate the numerical computation. Moreover, the previous numerical simulation (Zhang & Zou, 2023) has also been replaced by an experimental implementation in a 3-axis nanopositioning tracking. illustrating the proposed approach in a much more convincing manner.

2. Problem formulation

Consider a square MIMO linear time invariant (LTI) system given in the frequency domain

$$\mathbf{y}(j\omega) = \mathbf{G}(j\omega)\mathbf{u}(j\omega) + \mathbf{d}(j\omega),\tag{1}$$

where ' $j\omega$ ' denotes the Fourier transform of a time-domain signal, $\boldsymbol{G}(j\omega) \in \mathbb{C}^{p\times p}$ is the transfer function matrix (Skogestad & Postlethwaite, 2007) from the input $\boldsymbol{u}(j\omega) \in \mathbb{C}^{p\times 1}$ to the output $\boldsymbol{y}(j\omega) \in \mathbb{C}^{p\times 1}$, $\boldsymbol{d}(j\omega) \in \mathbb{C}^{p\times 1}$ is the output disturbance (e.g., measurement noise), respectively.

Remark 1. The proposed approach can be extended to non-square systems as an over- or under- actuated system can be converted into a square one (Oppenheimer, Doman, & Bolender, 2006; Schkoda, 2007; Yan et al., 2021).

Assumption 1. The desired trajectory in any given *i*th output channel contains a finite N_i number of frequencies, i.e., for any given $i = 1, 2 \cdots p$, the desired trajectory of the *i*th output channel $y_{i,d}(j\omega) = 0$, except at $\omega = \omega_{g,i}$, for $q = 1, 2, \dots, N_i$.

Such a desired trajectory of a finite discrete spectrum appears in many tracking applications in practice—Seldom are we asked to track a white-noise-like desired trajectory. Also, tracking a frequency component in the output becomes infeasible when its amplitude becomes too small—smaller than the random noise at that frequency. Thus, we assume that

Assumption 2. The output disturbance in all output channels are independent, random, and bounded in 1-norm,

$$\sup_{\omega} \|\mathbf{D}(j\omega)\|_{1} \triangleq \sup_{\omega} \sum_{i=1}^{p} |d_{i}(j\omega)| \leq \varepsilon_{n} < \infty, \tag{2}$$

where $\varepsilon_n \in \mathbb{R}^+$ is a constant, and $d_i(j\omega) \in \mathbb{C}$ is the output disturbance in the ith (1 < i < p) channel.

Definition 1 (*Effective Frequency*). $\omega_{q,t} \in \mathbb{S}_{a,t}$ is an effective frequency – the qth effective frequency in the tth channel for $q=1,2,\ldots,N_t$ and $t=1,2,\ldots,p$ – if the amplitude of the corresponding desired output $|y_{t,d}(j\omega_{q,t})| \geq \epsilon_Y \geq \varepsilon_n > 0$ for given positive constant ϵ_Y . $\mathbb{S}_{a,t}$ is the set of effective frequencies in the tth channel, and $\mathbb{S}_a \triangleq \bigcup_t \mathbb{S}_{a,t}$ is the set of all effective frequencies.

Below we order the effective frequencies in \mathbb{S}_a in the ascending order, i.e., $\omega_1 \leq \omega_2 \leq \cdots \omega_{N_q}$, where N_q is the number of effective frequencies in \mathbb{S}_a .

Assumption 3. The transfer function matrix of system (1), $G(j\omega)$, is proper, stable, and hyperbolic, i.e., for any $i, j \in \mathbb{N}^+$ (\mathbb{N}^+ : the set of the natural numbers), the corresponding transfer function, $g_{i,j}(j\omega) \in G(j\omega)$, is proper, stable and hyperbolic. Also, the transmission zeros (Skogestad & Postlethwaite, 2007) of system (1), $z_r s \in \mathbb{C}$ ($r \in \mathbb{N}^+$), do not overlap with any of the effective frequencies. i.e., $z_r \notin \mathbb{S}_q$ for any given zero z_r of system (1).

First, we format the input and output trajectory matrices needed in the proposed DDRO-ILC technique. For any given rth input–output channel $(r=1,2,\ldots,p)$, let the effective desired trajectory matrix, $\mathbf{Y}_{r,d}(\mathbb{S}_a) \in \mathbb{C}^{N_q \times N_q}$ $(1 \leq r \leq p)$, and the effective input and output matrix in the kth iteration, $\mathbf{U}_{r,k}(\mathbb{S}_a) \in \mathbb{C}^{N_q \times N_q}$ $(1 \leq r \leq p)$ and $\mathbf{Y}_{r,k}(\mathbb{S}_a) \in \mathbb{C}^{N_q \times N_q}$ $(1 \leq r \leq p)$, respectively, be given by:

$$\mathbf{Y}_{r,d}(\mathbb{S}_{a}) = \operatorname{diag}([y_{r,d}(j\omega_{1}) \cdots y_{r,d}(j\omega_{N_{q}})])_{N_{q} \times N_{q}},$$

$$\mathbf{Y}_{r,k}(\mathbb{S}_{a}) = \operatorname{diag}([y_{r,k}(j\omega_{1}) \cdots y_{r,k}(j\omega_{N_{q}})])_{N_{q} \times N_{q}},$$

$$\mathbf{U}_{r,k}(\mathbb{S}_{a}) = \operatorname{diag}([u_{r,k}(j\omega_{1}) \cdots u_{r,k}(j\omega_{N_{q}})])_{N_{q} \times N_{q}},$$
(3)

where $\operatorname{diag}\{v\}$ denotes a diagonal matrix with the diagonal entries given by the vector $v = [v_1 \ v_2 \ \cdots \ v_{N_q}]$. Then, the effective output tracking error matrix, $\boldsymbol{E}_k(\mathbb{S}_a)$, is given by

$$\begin{aligned} & \boldsymbol{E}_{k}(\mathbb{S}_{a}) = \boldsymbol{Y}_{d}(\mathbb{S}_{a}) - \boldsymbol{Y}_{k}(\mathbb{S}_{a}), & \text{where} \\ & \boldsymbol{Y}_{k}(\mathbb{S}_{a}) = \begin{bmatrix} \boldsymbol{Y}_{1,k}(\mathbb{S}_{a}) & \cdots & \boldsymbol{Y}_{p,k}(\mathbb{S}_{a}) \end{bmatrix}_{pN_{q} \times N_{q}}^{T} & \text{and} \\ & \boldsymbol{Y}_{d}(\mathbb{S}_{a}) = \begin{bmatrix} \boldsymbol{Y}_{1,d}(\mathbb{S}_{a}) & \cdots & \boldsymbol{Y}_{p,d}(\mathbb{S}_{a}) \end{bmatrix}_{pN_{q} \times N_{a}}^{T}, & k \geq 0, \end{aligned}$$

The effective input matrix in the kth iteration, $\boldsymbol{U}_k(\mathbb{S}_a)$, can be represented in terms of $\boldsymbol{U}_{i,k}(\mathbb{S}_a)$ (1 $\leq i \leq p$), similarly as the

above representation of the effective output matrix $\mathbf{Y}_k(\mathbb{S}_a)$ in $\mathbf{Y}_{i,k}(\mathbb{S}_a)$ (1 < i < p).

Thus, by using the above defined effective input and output matrix, the ILC algorithm can be represented as

$$\mathbf{U}_{k+1}(\mathbb{S}_a) = \mathcal{Q}_k(\mathbb{S}_a)\mathbf{U}_k(\mathbb{S}_a) + \mathbf{L}_k(\mathbb{S}_a)\mathbf{E}_k(\mathbb{S}_a), \ k \ge 1, \tag{5}$$

where $Q_k(\mathbb{S}_a)$, $L_k(\mathbb{S}_a) \in \mathbb{C}^{pN_q \times pN_q}$ are the corresponding effective low-pass filter and effective iteration gain matrix, respectively. Below we set $Q_k(\mathbb{S}_a) = I$ (I: an identity matrix of proper dimension) and focus on the design of $L_k(\mathbb{S}_a)$.

To further characterize the convergence of the proposed algorithm in practice, we define

Definition 2 (*Practically Monotonic Convergence*). A convergent sequence $\{a_n\}_{n=1}^{\infty}$ is practically monotonically convergent w.r.t. a given constant $\mathcal{Y} \in \mathbb{R}$, if

- (1) the set $\mathbb{A} = \{n | a_n \leq \mathcal{Y}\}$ is not empty, and
- (2) $a_n \le a_{n-1}$ for all $n \le n^*(\mathcal{Y})$, where $n^*(\mathcal{Y})$ is the least element of the set \mathbb{A} .

By the well ordering Theorem (Hungerford, 2012), $n^*(\mathcal{Y})$ always exists if condition 1 is satisfied. We now state the DDRO-ILC of MIMO systems.

DDRO-ILC OF LTI SYSTEMS For a LTI system given in Eq. (1), let Assumptions 1–3 hold, then the DDRO-ILC is to achieve the following objectives:

- \mathcal{P}_1 Construct and update the effective iteration gain matrix, $\mathbf{L}_k(\mathbb{S}_a)$, in each iteration by only using the input–output data acquired in the previous iteration.
- \mathcal{P}_2 Design the effective iteration gain matrix, $L_k(\mathbb{S}_a)$, such that
 - a Unbiased convergence is achieved, i.e.,

$$\lim_{k\to\infty} \|\boldsymbol{E}_k(\mathbb{S}_a)\|_2 \leq \mathcal{H}(\varepsilon_n),$$

where $\|\mathbf{V}\|_2$ denotes 2-norm of matrix \mathbf{V} , and $\mathcal{H}(\cdot)$: $\mathbb{R}_{\geq 0} \to \mathbb{R}_{\geq 0}$ ($\mathbb{R}_{\geq 0}$: the set of nonnegative real numbers) is a class κ function (Khalil, 2011) such that $\lim_{\varepsilon_n \to 0} \mathcal{H}(\varepsilon_n) = 0$.

b Practically monotonic convergence is reached w.r.t. $\mathcal{H}(\varepsilon_n)$, i.e., the set $\mathbb{A}=\{k|\ \|\pmb{E}_k(\mathbb{S}_a)\|_2\leq \mathcal{H}(\varepsilon_n)\}\neq\emptyset$, and

$$\|\mathbf{E}_k(\mathbb{S}_a)\|_2 < \|\mathbf{E}_{k-1}(\mathbb{S}_a)\|_2, \ k \leq k^*(\mathcal{H}(\varepsilon_n)),$$

where $k^*(\mathcal{H}(\varepsilon_n))$ is as $n^*(\mathcal{Y})$ in Definition 2.

 \mathcal{P}_3 Optimize the effective iteration gain matrix, $L_k(\mathbb{S}_a)$, such that the upper bound of the tracking error is minimized, and the convergence rate is maximized in the upper bound of the tracking error, i.e., find $L_k^*(\mathbb{S}_a)$, such that for any given effective frequency $\omega_a \in \mathbb{S}_a$ and any given iteration k,

$$\begin{split} \min_{\boldsymbol{L}_k(\mathbb{S}_a)} & \overline{\|\boldsymbol{E}_k(\mathbb{S}_a)\|}_2, \quad \text{and} \\ \max_{\boldsymbol{L}_k(\mathbb{S}_a)} & \left| \overline{\|\boldsymbol{E}_k(\mathbb{S}_a)\|}_2 - \overline{\|\boldsymbol{E}_{k-1}(\mathbb{S}_a)\|}_2 \right| \end{split}$$

are achieved, where $\overline{\|\mathbf{E}_k(\mathbb{S}_a)\|}_2$ is the upper bound of $\|\mathbf{E}_k(\mathbb{S}_a)\|_2$.

Thus by the above Objective \mathcal{P}_2 , we aim to achieve monotonic convergence in practical implementation, i.e., before the tracking error falls within the bound of $\mathcal{H}(\varepsilon_n)$ and the convergence is terminated, the tracking error is monotonically decreasing.

3. Data-driven robust iterative learning control

We present the proposed DDRO-ILC technique by showing the above three objectives in order. First, the effective iteration gain matrix $\boldsymbol{L}_k(\mathbb{S}_a)$ will be constructed by only using the previous input–output data (Objective \mathcal{P}_1).

3.1. DDRO-ILC algorithm

The proposed DDRO-ILC algorithm is given by

$$\mathbf{U}_{1}(\mathbb{S}_{a}) = \mathbb{U}^{int}(\mathbb{S}_{a})(\mathbb{Y}^{int}(\mathbb{S}_{a}))^{\dagger}\mathbf{Y}_{d}(\mathbb{S}_{a}), \qquad k = 1,
\mathbf{U}_{k}(\mathbb{S}_{a}) = \mathbf{U}_{k-1}(\mathbb{S}_{a}) + \Delta \mathbb{U}_{k-1,s}(\mathbb{S}_{a})(\Delta \mathbb{Y}_{k-1,s}(\mathbb{S}_{a}))^{\dagger}
\mathbf{\Phi}_{k-1}(\mathbb{S}_{a})\mathbf{E}_{k-1}(\mathbb{S}_{a}), \qquad k \geq 2,$$
(6)

where $\mathbb{U}^{int}(\mathbb{S}_a) \in \mathbb{C}^{pN_q \times pN_q}$ and $\mathbb{Y}^{int}(\mathbb{S}_a) \in \mathbb{C}^{pN_q \times pN_q}$ are the effective initialization input and output matrices, respectively:

$$\mathbb{U}^{int}(\mathbb{S}_a) = \begin{bmatrix} \boldsymbol{U}_1^{int}(\mathbb{S}_a) & \cdots & \boldsymbol{U}_p^{int}(\mathbb{S}_a) \end{bmatrix},
\mathbb{Y}^{int}(\mathbb{S}_a) = \begin{bmatrix} \boldsymbol{Y}_1^{int}(\mathbb{S}_a) & \cdots & \boldsymbol{Y}_p^{int}(\mathbb{S}_a) \end{bmatrix},$$
(7)

where $\boldsymbol{U}_i^{int}(\mathbb{S}_a) \in \mathbb{C}^{pN_q \times N_q}$ and $\boldsymbol{Y}_i^{int}(\mathbb{S}_a) \in \mathbb{C}^{pN_q \times N_q}$ are the Fourier transform of the ith effective initialization input and the corresponding output, respectively. As shown in Section 3.2, the initialization input, $\mathbb{U}_{int}(\mathbb{S}_a)$, is designed such that both the initialization input and the output matrices have full rank.

Moreover, in Eq. (6),

$$\Delta \mathbb{U}_{k,s}(\mathbb{S}_a) = \begin{bmatrix} \mathbb{U}^{int}(\mathbb{S}_a) & \Delta \mathbf{U}_k(\mathbb{S}_a) \end{bmatrix}_{pN_q \times ((p+1)N_q)},
\Delta \mathbb{Y}_{k,s}(\mathbb{S}_a) = \begin{bmatrix} \mathbb{Y}^{int}(\mathbb{S}_a) & \Delta \mathbf{Y}_k(\mathbb{S}_a) \end{bmatrix}_{pN_q \times ((p+1)N_q)},$$
(8)

witl

$$\Delta \boldsymbol{U}_k(\mathbb{S}_a) = \begin{cases} \boldsymbol{U}_1(\mathbb{S}_a) - \boldsymbol{U}_p^{int}(\mathbb{S}_a), & k = 1 \\ \boldsymbol{U}_k(\mathbb{S}_a) - \boldsymbol{U}_{k-1}(\mathbb{S}_a), & \text{otherwise} \end{cases},$$

$$\Delta \boldsymbol{Y}_k(\mathbb{S}_a) = \begin{cases} \boldsymbol{Y}_1(\mathbb{S}_a) - \boldsymbol{Y}_p^{int}(\mathbb{S}_a), & k = 1 \\ \boldsymbol{Y}_k(\mathbb{S}_a) - \boldsymbol{Y}_{k-1}(\mathbb{S}_a), & \text{otherwise} \end{cases},$$

and finally, $\Delta \mathbb{Y}_{k,s}^{\dagger}(\mathbb{S}_a)$ denotes the Moore–Penrose pseudoinverse of $\Delta \mathbb{Y}_{k,s}(\mathbb{S}_a)$, $\boldsymbol{\Phi}_k(\mathbb{S}_a) \in \mathbb{C}^{pN_q \times pN_q}$ is the iteration gain matrix to be designed, respectively.

Comparing Eq. (6) to Eq. (5) shows that in the proposed DDRO-ILC algorithm, the effective iteration gain matrix $L_k(\mathbb{S}_a)$ is given by

$$\mathbf{L}_{k}(\mathbb{S}_{a}) = \Delta \mathbb{U}_{k,s}(\mathbb{S}_{a}) \Delta \mathbb{Y}_{k,s}^{\dagger}(\mathbb{S}_{a}) \mathbf{\Phi}_{k}(\mathbb{S}_{a}).$$

Thus, $L_k(\mathbb{S}_a)$ is data-driven if the gain matrix $\Phi_k(\mathbb{S}_a)$ is designed by only using the previous input–output data. Towards that end we find the Moore–Penrose pseudoinverse of $\Delta \mathbb{Y}_{k,s}(\mathbb{S}_a)$ via the SVD (Horn & Johnson, 2012) as

$$\Delta \mathbb{Y}_{k,s}(\mathbb{S}_{a}) = \mathcal{U}_{k}(\mathbb{S}_{a}) \mathcal{Y}_{k}^{H}(\mathbb{S}_{a})
= \begin{bmatrix} \mathcal{U}_{1,k}(\mathbb{S}_{a}) & \mathcal{U}_{2,k}(\mathbb{S}_{a}) \end{bmatrix}
\begin{bmatrix} \mathcal{E}_{1,k}(\mathbb{S}_{a}) & \mathbf{0} \\ \mathbf{0} & \mathcal{E}_{2,k}(\mathbb{S}_{a}) \end{bmatrix} \begin{bmatrix} \mathcal{V}_{1,k}^{H}(\mathbb{S}_{a}) \\ \mathcal{V}_{2,k}^{H}(\mathbb{S}_{a}) \end{bmatrix}
= \mathcal{U}_{1,k}(\mathbb{S}_{a}) \mathcal{E}_{1,k}(\mathbb{S}_{a}) \mathcal{V}_{1,k}^{H}(\mathbb{S}_{a})
\triangleq \hat{\mathcal{U}}_{k}(\mathbb{S}_{a}) \hat{\mathcal{E}}_{k}(\mathbb{S}_{a}) \hat{\mathcal{V}}_{k}^{H}(\mathbb{S}_{a}),$$
(9)

where, respectively, $\mathcal{U}_k(\mathbb{S}_a)$ and $\mathcal{V}_k(\mathbb{S}_a)$ are unitary matrix, 'H' denotes the Hermitian transpose of the matrix, $\Sigma_k(\mathbb{S}_a)$ is the diagonal matrix containing all the singular values of $\Delta \mathbb{Y}_{k,s}(\mathbb{S}_a)$ in the descending order, $\Sigma_{1,k}(\mathbb{S}_a)$ and $\Sigma_{2,k}(\mathbb{S}_a)$ partition $\Sigma_k(\mathbb{S}_a)$ with nonzero and zero diagonal entries, i.e.,

$$\begin{split} \hat{\boldsymbol{\Sigma}}_k(\mathbb{S}_a) &= \boldsymbol{\varSigma}_{1,k}(\mathbb{S}_a) \\ &= \text{diag}\{[\sigma_1(\boldsymbol{\varSigma}_{1,k}(\mathbb{S}_a)), \ldots, \sigma_{N_\tau}(\boldsymbol{\varSigma}_{1,k}(\mathbb{S}_a))]\}, \\ &\quad \text{with} \quad \sigma_1(\boldsymbol{\varSigma}_{1,k}(\mathbb{S}_a)) \geq \cdots \geq \sigma_{N_\tau}(\boldsymbol{\varSigma}_{1,k}(\mathbb{S}_a)) > 0, \end{split}$$

where $\sigma_i(\mathbf{F})$ denotes the ith singular value of matrix \mathbf{F} , and $\hat{\mathcal{U}}_k(\mathbb{S}_a) = \mathcal{U}_{1,k}(\mathbb{S}_a)$ and $\hat{\mathcal{V}}_k(\mathbb{S}_a) = \mathcal{V}_{1,k}(\mathbb{S}_a)$ are partitions of $\mathcal{U}_k(\mathbb{S}_a)$ and $\mathcal{V}_k(\mathbb{S}_a)$ according to the dimension of $\Sigma_{1,k}$ and $\Sigma_{2,k}$, respectively. Then the pseudoinverse of $\Delta \mathbb{Y}_{k,s}(\mathbb{S}_a)$ is given by

$$\Delta \mathbb{Y}_{k,c}^{\dagger}(\mathbb{S}_a) = \hat{\mathcal{V}}_k(\mathbb{S}_a) \hat{\mathcal{L}}_k^{-1}(\mathbb{S}_a) \hat{\mathcal{U}}_k^H(\mathbb{S}_a). \tag{10}$$

The gain matrix $\Phi_k(\mathbb{S}_a)$ is chosen as

$$\Phi_{k}(\mathbb{S}_{a}) = \hat{\mathcal{U}}_{k}(\mathbb{S}_{a})\phi_{k}\hat{\mathcal{U}}_{k}^{H}(\mathbb{S}_{a}),$$
with $\phi_{k} = \rho_{k,1} \oplus \cdots \oplus \rho_{k,p}$, and
$$\rho_{k,i} = \operatorname{diag}([\varphi_{k,i}^{1}, \dots, \varphi_{k,i}^{F}, \dots, \varphi_{k,i}^{N_{q}}])_{N_{q} \times N_{q}},$$
for $i = 1, \dots, p, \ 1 \leq F \leq N_{q}$,
$$(11)$$

where \oplus denotes the direct sum operation of two matrices (Horn & Johnson, 2012), i.e., for $A \in \mathbb{C}^{m \times m}$ and $B \in \mathbb{C}^{n \times n}$, $A \oplus B = \operatorname{diag}([A\ B])_{(m+n)\times(m+n)}$, and $\varphi^F_{k,i}(\omega_j) \in \mathbb{R}^+$ (\mathbb{R}^+ : the set of positive real numbers). Then, the DDRO-ILC algorithm becomes

$$\mathbf{U}_{1}(\mathbb{S}_{a}) = \mathbb{U}^{int}(\mathbb{S}_{a})(\mathbb{Y}^{int}(\mathbb{S}_{a}))^{\dagger} \mathbf{Y}_{d}(\mathbb{S}_{a}), \qquad k = 1,
\mathbf{U}_{k}(\mathbb{S}_{a}) = \mathbf{U}_{k-1}(\mathbb{S}_{a}) + \Delta \mathbb{U}_{k-1,s}(\mathbb{S}_{a})(\Delta \mathbb{Y}_{k-1,s}(\mathbb{S}_{a}))^{\dagger}
\hat{\mathcal{U}}_{k-1}(\mathbb{S}_{a}) \boldsymbol{\phi}_{k-1} \hat{\mathcal{U}}_{k-1}^{H}(\mathbb{S}_{a}) \boldsymbol{E}_{k-1}(\mathbb{S}_{a}), \qquad k \geq 2.$$
(12)

Thus, in practice, the input-output data obtained after each iteration will be first pruned to only retain the effective frequency components, and then used to form the input and the output matrix as in Eqs. (3)–(4) to obtain the next-iteration input via Eq. (12). The choice of the iteration gain matrix to ensure the convergence is addressed later in Section 3.3. Next we discuss the initialization of the input-output matrix, $\mathbb{U}^{int}(\mathbb{S}_a)$ and $\mathbb{Y}^{int}(\mathbb{S}_a)$.

3.2. Input initialization

We proposed an initialization process by repetitively applying an initialization input $\boldsymbol{u}_{*,i}^{int}(t) \in \mathbb{R}^p$ to the system for p times, where each time the initialization input $\boldsymbol{u}_{*,i}^{int}(t)$ for $i=1,2,\ldots,p$ is in the form of

$$\mathbf{u}_{*,i}^{int}(t) = \begin{bmatrix} u_{1,i}^{int}(t) & u_{2,i}^{int}(t) & \cdots & u_{p,i}^{int}(t) \end{bmatrix}^T$$

with $u_{m,i}^{int}(t)$ $(1 \le m \le p)$ the input applied to the mth input channel, and the corresponding output $\boldsymbol{y}_{*,i}^{int}(t) \in \mathbb{R}^p$ (for $i=1,\ldots,p$) is measured. The input $\boldsymbol{u}_{*,i}^{int}(t)$ is designed to guarantee that the effective initialization input matrix, $\mathbb{U}^{int}(\mathbb{S}_a)$ given in Eq. (7), has full rank in the frequency domain, so is the initialization output matrix $\mathbb{Y}^{int}(\mathbb{S}_a)$ (by Assumption 3).

Specifically, in any given *i*th initialization, the input $\mathbf{u}_{*,i}^{int}(t)$ can be chosen as a chirp signal such that its Fourier transform, $\mathbf{U}_{i}^{int}(\mathbb{S}_{a})$, contains all the effective frequency components

$$\mathbf{U}_{i}^{int}(\mathbb{S}_{a}) = \begin{bmatrix} \boldsymbol{\Gamma}_{1,i}(\mathbb{S}_{a}) & \cdots & \boldsymbol{\Gamma}_{p,i}(\mathbb{S}_{a}) \end{bmatrix}_{pN_{q} \times N_{q}}^{T},
\text{for } i = 1, 2, \dots, p,$$
(13)

where

$$\Gamma_{m,i}(\mathbb{S}_a) = \operatorname{diag}\left(\left[u_{m,i}^{int}(j\omega_1) \quad \cdots \quad u_{m,i}^{int}(j\omega_{N_q})\right]\right)_{N_a \times N_a},$$
 (14)

for $m=1,2,\ldots,p$, i.e., the diagonal matrix $\Gamma_{m,i}(\mathbb{S}_a)$ has its diagonal elements given by the effective frequency components of $u_{m,i}^{int}(t)$. Below we give the condition that guarantees the full rank of the initialization input $\mathbb{U}^{int}(\mathbb{S}_a)$.

Lemma 1. The initialization input matrix $\mathbb{U}^{int}(\mathbb{S}_a)$ is full rank if and only if the following matrix $\Psi(\omega_l) \in \mathbb{C}^{p \times p}$

$$\boldsymbol{\varPsi}(\omega_l) = \begin{bmatrix} u_{1,1}^{int}(j\omega_l) & \cdots & u_{1,p}^{int}(j\omega_l) \\ \vdots & \ddots & \vdots \\ u_{p,1}^{int}(j\omega_l) & \cdots & u_{p,p}^{int}(j\omega_l) \end{bmatrix}_{p \times p},$$

is nonsingular for $l = 1, ..., N_a$.

Proof. See Appendix A □

As an example, the initialization input $u_{m,i}^{int}(t)$ satisfying Lemma 1 can be designed as a chirp signal as,

$$u_{m,i}^{int}(t) = \begin{cases} \alpha_{m,i} \sin(\omega_{b(t)}t), & \text{when } m = i, \\ 0, & \text{otherwise.} \end{cases}$$
with
$$\omega_{b(t)} \in \mathbb{S}_a, \ b(t) = \left(\frac{t}{t} \bmod N_q\right) + 1,$$
(15)

where $\alpha_{m,i} \in \mathbb{R}^+$ is a constant, t_s is the time for each step, and 'mod' denotes modulo operation (Lin, Lee, & Chang, 2009).

Remark 2. For single-input single-output (SISO) systems, the DDRO-ILC algorithm is reduced to the data-driven difference-inversion-based iterative control (DDD-IC) method in Wang and Zou (2023), where the initiation matrix is simplified to a constant.

3.3. Convergence analysis

Next, we show the convergence of the proposed DDRO-ILC technique (Objective \mathcal{P}_2), by finding a recursive form of the iterative tracking error first.

Lemma 2. Let Assumptions 1–3 hold, then the propagation of the iterative tracking error is given by:

$$\mathbf{E}_{k}(\mathbb{S}_{a}) = \boldsymbol{\beta}_{k-1}(\mathbb{S}_{a})\mathbf{E}_{k-1}(\mathbb{S}_{a}) - \Delta \mathbf{D}_{k}(\mathbb{S}_{a}),$$

where

$$\begin{aligned} \boldsymbol{\beta_{k-1}}(\mathbb{S}_a) &= \boldsymbol{I} - (\Delta \mathbb{Y}_{k-1,s}(\mathbb{S}_a) - \Delta \mathbb{D}_{k-1,s}(\mathbb{S}_a)) \\ & (\Delta \mathbb{Y}_{k-1,s}(\mathbb{S}_a))^{\dagger} \boldsymbol{\mathcal{U}}_{k-1}(\mathbb{S}_a) \boldsymbol{\phi}_{k-1} \boldsymbol{\mathcal{U}}_{k-1}^{H}(\mathbb{S}_a), \\ \Delta \boldsymbol{D}_k(\mathbb{S}_a) &= \begin{cases} \boldsymbol{D}_1(\mathbb{S}_a) - \boldsymbol{D}_p^{int}(\mathbb{S}_a), & k = 1 \\ \boldsymbol{D}_k(\mathbb{S}_a) - \boldsymbol{D}_{k-1}(\mathbb{S}_a), & otherwise \end{cases}, \end{aligned}$$

with

$$\Delta \mathbb{D}_{k,s}(\mathbb{S}_{a}) = \begin{bmatrix} \mathbb{D}^{int}(\mathbb{S}_{a}) & \Delta \mathbf{D}_{k}(\mathbb{S}_{a}) \end{bmatrix}_{pN_{q} \times ((p+1)N_{q})},
\mathbb{D}^{int}(\mathbb{S}_{a}) = \begin{bmatrix} \mathbf{D}_{1}^{int}(\mathbb{S}_{a}) & \cdots & \mathbf{D}_{p}^{int}(\mathbb{S}_{a}) \end{bmatrix}_{pN_{q} \times pN_{q}},
\mathbf{D}_{k}(\mathbb{S}_{a}) = \begin{bmatrix} \mathbf{D}_{k,1}(\mathbb{S}_{a}) & \cdots & \mathbf{D}_{k,p}(\mathbb{S}_{a}) \end{bmatrix}^{T},
\mathbf{D}_{r,k} = \operatorname{diag} \begin{bmatrix} d_{k,r}(j\omega_{1}) & \cdots & d_{k,r}(j\omega_{N_{q}}) \end{bmatrix},
for $r = 1, 2, \dots, p$.
(16)$$

where $\mathbf{D}_{i}^{int}(\mathbb{S}_{a}) \in \mathbb{C}^{pN_{q} \times N_{q}}$ is the output disturbance occurred in the ith $(1 \leq i \leq p)$ initialization process.

Lemma 2 can be shown by writing the effective iteration tracking error $E_k(\mathbb{S}_a)$ in the matrix form using the system in Eq. (1), and presenting the iterative control input $U_k(\mathbb{S}_a)$ by the proposed DDRO-ILC in Eq. (12). The complete proof is omitted to save space.

Next, considering the effect of random output disturbance, we assume that

Assumption 4. The gain of the system at effective frequencies is bounded below by the disturbance as

$$\underline{h}_g \triangleq \min_{\substack{\omega \in \mathbb{S}_a \\ 1 \leq i \leq p}} \sigma_i(\boldsymbol{G}(j\omega)) > \frac{(\sqrt{6}+1)\varepsilon_n}{\alpha},$$

with

$$\alpha \triangleq \sigma_{pN_a}(\mathbb{U}^{int}(\mathbb{S}_a)) > 0.$$
 (17)

Remark 3. The above Assumption 4 is to ensure that the response to a given input is large enough such that the output is not dominant and swallowed by disturbance. Also, in practice, the amplitude of the initialization input $\mathbb{U}^{int}(\mathbb{S}_a)$ can be adjusted to satisfy Assumption 4.

Lemma 3. Let Assumptions 1–4 be satisfied, then in any given kth iteration.

(1) The output disturbance is bounded as

$$\|\Delta \mathbb{D}_{k,s}(\mathbb{S}_{q})\|_{2} < \sqrt{6}\varepsilon_{n},$$

and initially (i.e., k = 0)

$$\|\mathbb{D}^{int}(\mathbb{S}_a)\|_2 \le \varepsilon_n. \tag{18}$$

(2) The pseudo-inverse of the effective output difference $(\Delta \Psi_{k,s}(\mathbb{S}_a))^{\dagger}$ is bounded above by

$$\|(\Delta \mathbb{Y}_{k,s}(\mathbb{S}_a))^{\dagger}\|_2 \leq \frac{1}{\alpha \underline{h}_g - \varepsilon_n} < \frac{1}{\sqrt{6}\varepsilon_n}.$$

Proof. By Eq. (16) and the definition of induced matrix 1- and ∞ - norm (Horn & Johnson, 2012),

$$\|\Delta \mathbb{D}_{k,s}(\mathbb{S}_a)\|_1 = \sup_{\substack{1 \le q \le N_q \\ 1 \le r \le p}} \left\{ \sum_{i=1}^p |d_r^{int}(j\omega_{q,i})|, \quad \sum_{i=1}^p |\Delta d_{k,i}(j\omega_q)| \right\}$$

$$\|\Delta \mathbb{D}_{k,s}(\mathbb{S}_a)\|_{\infty} = \sup_{\substack{1 \leq q \leq N_q \\ 1 \leq i \leq p}} \left\{ \sum_{r=1}^p |d_r^{int}(j\omega_{q,i})| + |\Delta d_{k,i}(j\omega_q)| \right\}$$

where

$$\Delta d_k(j\omega_{q,i}) = \begin{cases} d_{1,i}(j\omega_q) - d_p^{int}(j\omega_{q,i}), & \text{when } k = 1 \\ d_{k,i}(j\omega_q) - d_{k-1,i}(j\omega_q), & \text{when } k \ge 2 \end{cases}$$

and $d_r^{int}(j\omega_{q,i})$ and $d_{k,i}(j\omega_q)$ are the output disturbance at the qth effective frequency in the ith output channel, occurring during the rth initialization and kth iteration, respectively. Thus by Assumption 2 (Eq. (2)),

$$\begin{split} \|\Delta \mathbb{D}_{k,s}(\mathbb{S}_a)\|_1 &\leq \sup_{\substack{1 \leq q \leq N_q \\ 1 \leq r \leq p}} \left\{ \sum_{i=1}^p |d_r^{int}(j\omega_{q,i})|, \\ \sum_{i=1}^p |d_{k,i}(j\omega_q)| + \sum_{i=1}^p |d_{k-1,i}(j\omega_q)| \right\} \\ &\leq 2\varepsilon_n \end{split}$$

Similarly, it can be verified that $\|\Delta \mathbb{D}_{k,s}(\mathbb{S}_a)\|_{\infty} \leq 3\varepsilon_n$. Thus, by the property of matrix 2-norm (Horn & Johnson, 2012),

$$\|\Delta \mathbb{D}_{k,s}(\mathbb{S}_a)\|_2 \leq \sqrt{\|\Delta \mathbb{D}_{k,s}(\mathbb{S}_a)\|_1 \|\Delta \mathbb{D}_{k,s}(\mathbb{S}_a)\|_{\infty}} \leq \sqrt{6\varepsilon_n}$$

The upper bound of $\|\mathbb{D}^{int}(\mathbb{S}_a)\|_2$ can be verified similarly.

To quantify the lower-bound of $\Delta \mathbb{Y}_{k,s}^{\dagger}(\mathbb{S}_a)$, we note that the full row rank condition of $\mathbb{Y}^{int}(\mathbb{S}_a)$ implies that

$$\|\Delta \mathbb{Y}_{k,s}^{\dagger}(\mathbb{S}_a)\|_2 = \frac{1}{\sigma_{pN_a}(\Delta \mathbb{Y}_{k,s}(\mathbb{S}_a))},\tag{19}$$

where $\sigma_{pN_q}(\mathbb{Y}_{k,s}(\mathbb{S}_a))$ is the least singular value of $\mathbb{Y}_{k,s}(\mathbb{S}_a)$. As $\mathbb{Y}^{int}(\mathbb{S}_a)$ is nonsingular and by Eq. (8),

$$\sigma_{pN_q}(\Delta \mathbb{Y}_{k,s}(\mathbb{S}_a)) = \sigma_{pN_q} \left(\begin{bmatrix} \mathbb{Y}^{int}(\mathbb{S}_a) & \Delta \mathbf{Y}_k(\mathbb{S}_a) \end{bmatrix} \right)$$

$$\geq \sigma_{pN_q}(\mathbb{Y}^{int}(\mathbb{S}_a))$$
(20)

Then, by the definition of the least singular value and the triangle inequality (Horn & Johnson, 2012), $\sigma_{vNa}(\mathbb{Y}^{int}(\mathbb{S}_a))$ is bounded

below as

$$\sigma_{pN_q}(\mathbb{Y}^{int}(\mathbb{S}_a)) = \sigma_{pN_q}(\mathcal{G}(\mathbb{S}_a)\mathbb{U}^{int}(\mathbb{S}_a) + \mathbb{D}^{int}(\mathbb{S}_a))$$

$$\geq \min_{\|\mathbf{x}\|_1 = 1} \left| \|\mathcal{G}(\mathbb{S}_a)\mathbb{U}^{int}(\mathbb{S}_a)\mathbf{x}\|_2 - \|\mathbb{D}^{int}(\mathbb{S}_a)\mathbf{x}\|_2 \right|$$
(21)

where

$$\mathcal{G}(\mathbb{S}_a) = \begin{bmatrix} \mathcal{B}_{1,1}(\mathbb{S}_a) & \cdots & \mathcal{B}_{1,p}(\mathbb{S}_a) \\ \vdots & \ddots & \vdots \\ \mathcal{B}_{p,1}(\mathbb{S}_a) & \cdots & \mathcal{B}_{p,p}(\mathbb{S}_a) \end{bmatrix}_{pN_a \times pN_a}$$
(22)

witl

$$\mathcal{B}_{\ell,g}(\mathbb{S}_a) = \operatorname{diag}\left(\left[G_{\ell,g}(j\omega_1)\cdots G_{\ell,g}(j\omega_{N_q})\right]\right)_{N_a \times N_a}.$$
 (23)

Next, we quantify the lower bound of the right-hand side of the last inequality above. As $\mathcal{G}(\mathbb{S}_a)$ is nonsingular, by the property of singular value (Horn & Johnson, 2012) and Eq. (17), the least singular value of $\mathcal{G}(\mathbb{S}_a)\mathbb{U}^{int}(\mathbb{S}_a)$ is bounded as

$$egin{aligned} \sigma_{pN_q}(\mathcal{G}(\mathbb{S}_a)\mathbb{U}^{int}(\mathbb{S}_a)) &\geq \sigma_{pN_q}(\mathcal{G}(\mathbb{S}_a))\sigma_{pN_q}(\mathbb{U}^{int}(\mathbb{S}_a)) \ &= lpha\sigma_{pN_q}(\mathcal{G}(\mathbb{S}_a)) \end{aligned}$$

By Eq. (22), (23), $\mathcal{G}(\mathbb{S}_a)$ has the same structure as $\mathbb{U}^{int}(\mathbb{S}_a)$. By the permutation process in Eq. (A.1), (A.2), the following matrix $\mathbb{G}(\mathbb{S}_a)$

$$\mathbb{G}(\mathbb{S}_a) = \mathbb{B}_{p,N_q} \mathcal{G}(\mathbb{S}_a) \mathbb{B}_{p,N_q}^T,$$

is block diagonal with

$$\mathbb{G}(\mathbb{S}_a) = \mathbf{G}(j\omega_1) \oplus \mathbf{G}(j\omega_2) \cdots \oplus \mathbf{G}(j\omega_{N_a}).$$

therefore the block diagonal structure of $\mathbb{G}(\mathbb{S}_q)$ above implies that

$$\sigma_{pN_q}(\mathcal{G}(\mathbb{S}_a)) = \sigma_{pN_q}(\mathbb{G}(\mathbb{S}_a)) = \min_{\substack{\omega \in \mathbb{S}_a \ 1 \leq i \leq p}} \sigma_i(G(j\omega)).$$

Combining with Assumption 4 and Eq. (18) leads to

$$\alpha \sigma_{pN_q}(\mathcal{G}(\mathbb{S}_a)) > \varepsilon_n \ge \|\mathbb{D}^{int}(\mathbb{S}_a)\|_2.$$
 (24)

Thus, Eq. (24) implies that

$$\min_{\|\mathbf{x}\|_{2}=1} \|\mathbf{\mathcal{G}}(\mathbb{S}_{a})\mathbb{U}^{int}(\mathbb{S}_{a})\mathbf{x}\|_{2} > \max_{\|\mathbf{x}\|_{2}=1} \|\mathbb{D}^{int}(\mathbb{S}_{a})\mathbf{x}\|_{2}, \tag{25}$$

and combining Eq. (20), (24), (25) with Eq. (21) leads to

$$\sigma_{pN_q}(\Delta \mathbb{Y}_{k,s}(\mathbb{S}_a)) \ge \sigma_{pN_q}(\mathbb{Y}^{int}(\mathbb{S}_a)) \ge \alpha \underline{h}_g - \varepsilon_n > \sqrt{6}\varepsilon_n. \tag{26}$$

Thus, the proof is completed by substituting Eq. (26) into Eq. (19). $\ \ \Box$

Theorem 1 (Convergence condition). At any given frequency $\omega_a \in \mathbb{S}_a$, let Assumptions 1–4 be satisfied, and let the iteration gain, $\varphi_{k,i}^j$, for $i=1,\ldots,p$ and $j=1,\ldots,N_q$ be chosen as,

$$0 < \varphi_{k,i}^j < \frac{2}{1+\Omega} < 2, \tag{27}$$

where $\Omega \in (0, 1)$ is a finite constant defined as

$$\Omega = \frac{\sqrt{6}\varepsilon_n}{\alpha \underline{h}_{\sigma} - \varepsilon_n},\tag{28}$$

then, the DDRO-ILC algorithm converges,

$$\lim_{k \to \infty} \|\boldsymbol{E}_k(\mathbb{S}_a)\|_2 < \frac{2\varepsilon_n}{1 - \overline{\eta}} \triangleq \mathcal{H}(\varepsilon_n), \tag{29}$$

where the constant $\overline{\eta}$

$$\overline{\eta} \triangleq \max_{i,j,k} \left\{ |1 - \varphi_{k,i}^j| + \Omega \varphi_{k,i}^j \right\} \tag{30}$$

satisfies
$$0 < \overline{\eta} < 1$$
, for $1 \le j \le N_a$, $1 \le i \le p$.

Proof. By Lemma 2 and the triangle inequality,

$$\|\boldsymbol{E}_{k}(\mathbb{S}_{a})\|_{2} \leq \|\boldsymbol{\beta}_{k-1}(\mathbb{S}_{a})\|_{2} \|\boldsymbol{E}_{k-1}(\mathbb{S}_{a})\|_{2} + \|\Delta \boldsymbol{D}_{k}(\mathbb{S}_{a})\|_{2}$$

$$\leq (\psi_{k-1}(\mathbb{S}_{a}) + \zeta_{k-1}(\mathbb{S}_{a})) \|\boldsymbol{E}_{k-1}(\mathbb{S}_{a})\|_{2}$$

$$+ \|\Delta \boldsymbol{D}_{k}(\mathbb{S}_{a})\|_{2},$$
(31)

where

$$\psi_{k-1}(\mathbb{S}_a) = \|\mathbf{I} - \Delta \mathbb{Y}_{k-1,s}(\mathbb{S}_a)(\Delta \mathbb{Y}_{k-1,s}(\mathbb{S}_a))^{\dagger} \boldsymbol{\Phi}_{k-1}(\mathbb{S}_a)\|_{2},
\zeta_{k-1}(\mathbb{S}_a) = \|\Delta \mathbb{D}_{k-1,s}(\mathbb{S}_a)\Delta \mathbb{Y}_{k-1,s}^{\dagger}(\mathbb{S}_a)\boldsymbol{\Phi}_{k-1}(\mathbb{S}_a)\|_{2}.$$
(32)

To seek the bound of the iteration gain $\varphi_{k,i}^j$ to guarantee the convergence, we expand the effective initialization matrix via SVD in Eq. (9). Then, substituting the decomposition results and Eq. (11) into Eq. (32) yields

$$\psi_{k-1}(\mathbb{S}_a) = \|\mathbf{I} - \mathbf{\Phi}_{k-1}(\mathbb{S}_a)\|_2 \le \max_{i,j,k} \left\{ |1 - \varphi_{k,i}^j| \right\},\tag{33}$$

and

$$\zeta_{k-1}(\mathbb{S}_a) \leq \|\Delta \mathbb{D}_{k-1,s}(\mathbb{S}_a)\|_2 \|\Delta \mathbb{Y}_{k-1,s}^{\dagger}(\mathbb{S}_a)\|_2 \|\underline{\boldsymbol{\Phi}}_{k-1}(\mathbb{S}_a)\|_2 \\
\leq \|\Delta \mathbb{D}_{k-1,s}(\mathbb{S}_a)\|_2 \|\Delta \mathbb{Y}_{k-1,s}^{\dagger}(\mathbb{S}_a)\|_2 |\underline{\boldsymbol{\varphi}}_{k-1,i}^{j}|, \tag{34}$$

for $1 \le j \le N_q$, $1 \le i \le p$, where

$$\overline{|\varphi_{k,i}^j|} \triangleq \max_{i,i,k} \left\{ |\varphi_{k,i}^j| \right\}.$$

Substituting Eq. (33), (34) back into Eq. (31) leads to

$$\|\boldsymbol{E}_{k}(\mathbb{S}_{a})\|_{2} < \left(\overline{|1 - \varphi_{k-1,i}^{j}|} + \frac{\sqrt{6}\varepsilon_{n}}{\alpha \underline{h}_{g} - \varepsilon_{n}} \overline{|\varphi_{k-1,i}^{j}|}\right)$$

$$\|\boldsymbol{E}_{k-1}(\mathbb{S}_{a})\|_{2} + 2\varepsilon_{n}$$

$$\leq \overline{\eta} \|\boldsymbol{E}_{k-1}(\mathbb{S}_{a})\|_{2} + 2\varepsilon_{n}$$
(35)

where by Assumption 4, $\Omega \in (0, 1)$. Thus the convergence is guaranteed by choosing the iterative gain as in Eq. (27). This can be seen as when $\varphi_{k,i}^{j} \in (0, 1]$,

$$\overline{\eta} = \max_{i,j,k} \left\{ 1 - \varphi_{k,i}^j + \Omega \varphi_{k,i}^j \right\} < 1,$$

for $\Omega > 1$, $1 \le j \le N_q$, $1 \le i \le p$. Otherwise when $\varphi^j_{k,i} \in (1,2/(1+\Omega))$,

$$\begin{split} \overline{\eta} &= \max_{i,j,k} \left\{ -1 + (1+\Omega) \varphi_{k,i}^j \right\} \\ &< \max_{i,j,k} \left\{ -1 + (1+\Omega) \frac{2}{1+\Omega} \right\} = 1, \end{split}$$

for $1 \le j \le N_q$, $1 \le i \le p$. Thus, at the limit,

$$\lim_{k\to\infty} \|\boldsymbol{E}_k(\mathbb{S}_a)\|_2 \le \lim_{k\to\infty} \left\{ \overline{\eta}^{k-1} \|\boldsymbol{E}_1(\mathbb{S}_a)\|_2 + \frac{1-\overline{\eta}^{k-1}}{1-\overline{\eta}} 2\varepsilon_n \right\}$$
$$= \frac{2\varepsilon_n}{1-\overline{\eta}} \triangleq \mathcal{H}(\varepsilon_n).$$

Clearly the above function $\mathcal{H}(\varepsilon_n)$ is a κ function in ε , and $\lim_{\varepsilon_n \to 0} \mathcal{H}(\varepsilon_n) = 0$. This completes the proof. \square

Next we show that the proposed DDRO-ILC algorithm achieves the practically monotonic convergence.

Corollary 1 (Practically Monotonic Convergence). Let the conditions in Theorem 1 be satisfied, and let the iteration gain be chosen by Eq. (27), then the DDRO-ILC algorithm achieves practically monotonic convergence.

Proof. See Appendix B. \Box

Three observations are readily in place:

- Both the final tracking error and the convergence rate depend on the choice of the iterative gain $\varphi_{k,i}^j$: As the iterative gain $\varphi_{k,i}^j$ decreases towards zero, the inverse of the convergence rate $\overline{\eta}$ approaches to 1 (see Eq. (30)), resulting in a slow convergence and a large residual tracking error (see Eq. (29)). This agrees with our expectation as smaller iterative gain invites more disturbances accumulated in the output during the iterations, and thereby, larger tracking error.
- Theorem 1 also reveals that the tracking performance can be improved by increasing the system gain or choosing a larger initialization input $U_{int,i}(\mathbb{S}_a)$, i.e., a larger \underline{h}_g or α will lead to a larger lower bound of the minimal system gain, then a smaller constant Ω in Eq. (28)), and thereby, a faster convergence and a smaller residual tracking error. This observation motivates us to seek an optimal choice of the iteration gain matrix ϕ_k^* —Objective \mathcal{P}_3 .
- As a frequency-domain approach, the DDRO-ILC technique can account for the non-minimum phase dynamics effect, as the entire output trajectory is utilized in generating the iterative input (Devasia & Paden, 1998).

3.4. Iterative gain optimization

Corollary 2. Let the conditions in Theorem 1 be satisfied, and let the iteration gain matrix be chosen as $\phi_{\nu}^* = I$, then

(1) the upper bound of the residual error is minimized, i.e.,

$$\lim_{k\to\infty} \|\mathbf{E}_k(\mathbb{S}_a)\|_2 \le \frac{2\varepsilon_n}{1-\eta^*} \le \frac{2\varepsilon_n}{1-\overline{\eta}} \quad (\eta^* = \Omega),$$

(2) the convergence rate is maximized for the upper bound of the tracking error, i.e., $\eta^* < \overline{\eta}$ when $\phi_{\nu} \neq \phi_{\nu}^*$.

The Corollary can be shown by considering two cases: 1). $0 < \varphi_{k,i}^j \le 1$ for $1 \le j \le N_q$, $1 \le i \le p$, and $\overline{\eta} = \max_{i,j,k} \left\{1 - \varphi_{k,i}^j + \Omega \varphi_{k,i}^j\right\}$, and 2). $\varphi_{k,i}^j \ge 1$, for $1 \le j \le N_q$, $1 \le i \le p$, and $\overline{\eta} = \max_{i,j,k} \left\{\varphi_{k,i}^j - 1 + \Omega \varphi_{k,i}^j\right\}$, and showing that in both cases the minimal value is attained by setting $\varphi_{k,i}^j = 1$ for all $1 \le j \le N_q$, $1 \le i \le p$ and $k \in \mathbb{N}^+$. The proof is omitted due to space limit.

In practice, a non-unit iterative gain can be chosen to account for input saturation and noise-disturbance, e.g., the gain shall be reduced when the input amplitude is close to the saturation limit and increased when the input amplitude is close to the noise level.

3.5. Fast numerical computation

When implementing the proposed DDRO-ILC algorithm to high-dimension systems to track trajectories of rich frequency components, finding the pseudoinverse of the output difference matrix $\Delta \mathbb{Y}_{k,s}(\mathbb{S}_a)$ can be computationally intensive, as the computation complexity of $\Delta \mathbb{Y}_{k,s}^{\dagger}(\mathbb{S}_a)$ via SVD (by using, e.g., the optimized DGESVD (Anderson et al., 1999)) is at $\mathcal{O}(p(p+1)^2N_q^3)$. Next, we propose an algorithm to accelerate the computation.

By Eq. (8), (7), $\Delta \mathbb{Y}_{k,s}(\mathbb{S}_a)$ can be rewritten as

$$\Delta \mathbb{Y}_{k,s}(\mathbb{S}_{a}) = \begin{bmatrix} \mathbf{Y}_{1}^{int}(\mathbb{S}_{a}) & \cdots & \mathbf{Y}_{p}^{int}(\mathbb{S}_{a}) & \Delta \mathbf{Y}_{k}(\mathbb{S}_{a}) \end{bmatrix} \\
= \begin{bmatrix} \mathbf{\Upsilon}_{1,1}(\mathbb{S}_{a}) & \cdots & \mathbf{\Upsilon}_{1,p}(\mathbb{S}_{a}) & \Delta \mathbf{Y}_{1,k}(\mathbb{S}_{a}) \\ \vdots & \ddots & \vdots & \vdots \\ \mathbf{\Upsilon}_{p,1}(\mathbb{S}_{a}) & \cdots & \mathbf{\Upsilon}_{p,p}(\mathbb{S}_{a}) & \Delta \mathbf{Y}_{p,k}(\mathbb{S}_{a}) \end{bmatrix}, \text{ with}$$
(36)

$$\begin{split} \boldsymbol{\varUpsilon}_{n,i}(\mathbb{S}_a) &= \operatorname{diag}\left(\left[y_{n,i}^{int}(j\omega_1) \quad \cdots \quad y_{n,i}^{int}(j\omega_{N_q})\right]\right)_{N_q \times N_q}, \\ \Delta \boldsymbol{\varUpsilon}_{m,k}(\mathbb{S}_a) &= \begin{cases} \boldsymbol{\varUpsilon}_{m,k}(\mathbb{S}_a) - \boldsymbol{\varUpsilon}_{m,p}(\mathbb{S}_a), & \text{when } k = 1, \\ \boldsymbol{\varUpsilon}_{m,k}(\mathbb{S}_a) - \boldsymbol{\varUpsilon}_{m,k-1}(\mathbb{S}_a), & \text{when } k \geq 2, \end{cases} \\ &\text{for } m = 1, \ldots, p. \end{split}$$

where $\mathbf{Y}_{j,i}(\mathbb{S}_a)$ is diagonal as defined in Eq. (3). Then, by matrix permutation, $\Delta \mathbb{Y}_{k,s}(\mathbb{S}_a)$ in Eq. (36) can be transformed into a block matrix $\mathbb{L}_{k,s}(\mathbb{S}_a) \in \mathbb{C}^{pN_q \times (p+1)N_q}$, i.e,

$$\mathbb{L}_{k,s}(\mathbb{S}_a) = \mathbf{P}_a \Delta \mathbb{Y}_{k,s}(\mathbb{S}_a) \mathbf{P}_b,$$

= $\mathbf{M}_k(\omega_1) \oplus \mathbf{M}_k(\omega_2) \cdots \oplus \mathbf{M}_k(\omega_{N_a}),$ (37)

where $P_a \in \mathbb{R}^{pN_q \times pN_q}$ and $P_b \in \mathbb{R}^{(p+1)N_q \times (p+1)N_q}$ are the corresponding permutation matrices (Horn & Johnson, 2012), and matrix $M_k(\omega_l) \in \mathbb{C}^{p \times (p+1)}$ is given by

$$\mathbf{M}_{k}(\omega_{l}) = \begin{bmatrix} y_{1,1}^{int}(j\omega_{l}) & \cdots & y_{1,p}^{int}(j\omega_{l}) & | \\ \vdots & \ddots & \vdots & v_{k}(\omega_{l}) \\ y_{p,1}^{int}(j\omega_{l}) & \cdots & y_{p,p}^{int}(\omega_{l}) & | \end{bmatrix}_{p\times(p+1)},$$

$$\text{for } l = 1, \dots, N_{q}, \text{ with}$$

$$v_{k}(\omega_{l}) = \begin{bmatrix} v_{1,k}(\omega_{l}) & \cdots & v_{p,k}(\omega_{l}) \end{bmatrix}^{T}, \text{ and}$$

$$v_{r,k}(\omega_{l}) = \begin{cases} y_{r,k}(j\omega_{l}) - y_{r,p}^{int}(j\omega_{l}), & \text{when } k = 1, \\ y_{r,k}(j\omega_{l}) - y_{r,k-1}(j\omega_{l}), & \text{when } k \geq 2, \end{cases}$$

$$\text{for } r = 1, \dots, n \text{ the sum } p \text{ the }$$

where $y_{r,k}(j\omega_l)$ is defined in Eq. (3). Therefore, the SVD of matrix $\Delta \Psi_{k,s}(\mathbb{S}_a)$ can be replaced by SVD of matrix $\mathbf{M}_k(\omega_l)$ s of a much smaller size. By Eq. (37),

$$\Delta \mathbb{Y}_{k,s}(\mathbb{S}_a) = \boldsymbol{P}_{\boldsymbol{a}}^H \mathbb{L}_{k,s}(\mathbb{S}_a) \boldsymbol{P}_{\boldsymbol{b}}^H$$

$$= \boldsymbol{P}_{\boldsymbol{a}}^H (\boldsymbol{M}_k(\omega_1) \oplus \boldsymbol{M}_k(\omega_2) \cdots \oplus \boldsymbol{M}_k(\omega_{N_q})) \boldsymbol{P}_{\boldsymbol{b}}^H$$
and the SVD of $\boldsymbol{M}_k(\omega_l)$ is given by
$$\boldsymbol{M}_k(\omega_l) = U_{l,k}(\omega_l) S_{l,k}(\omega_l) V_{l,k}^H(\omega_l), \quad 1 \le l \le N_a.$$

Thus, the SVD of $\Delta \mathbb{Y}_{k,s}(\mathbb{S}_a)$ can be obtained as

$$\Delta \Psi_{k,s}(\mathbb{S}_{a}) = \mathbf{P}_{a}^{H} \mathfrak{U}_{k}(\mathbb{S}_{a}) \mathfrak{S}_{k}(\mathbb{S}_{a}) \mathfrak{V}_{k}^{H}(\mathbb{S}_{a}) \mathbf{P}_{b}^{H}
= \mathbf{P}_{a}^{H} \mathfrak{U}_{k}(\mathbb{S}_{a}) \mathfrak{S}_{k}(\mathbb{S}_{a}) \mathbf{P}_{c} \mathbf{P}_{c}^{H} \mathfrak{V}_{k}^{H}(\mathbb{S}_{a}) \mathbf{P}_{b}^{H}
= \mathcal{U}_{k}(\mathbb{S}_{a}) \mathcal{\Sigma}_{k}(\mathbb{S}_{a}) \mathcal{V}_{k}^{H}(\mathbb{S}_{a}), \text{ with}
\mathfrak{U}_{k}(\mathbb{S}_{a}) = U_{1,k}(\omega_{1}) \oplus U_{2,k}(\omega_{2}) \cdots \oplus U_{N_{q},k}(\omega_{N_{q}}),
\mathfrak{S}_{k}(\mathbb{S}_{a}) = S_{1,k}(\omega_{1}) \oplus S_{2,k}(\omega_{2}) \cdots \oplus S_{N_{q},k}(\omega_{N_{q}}),
\mathfrak{V}_{k}(\mathbb{S}_{a}) = V_{1,k}(\omega_{1}) \oplus V_{2,k}(\omega_{2}) \cdots \oplus V_{N_{q},k}(\omega_{N_{q}}),
\mathcal{U}_{k}(\mathbb{S}_{a}) = \mathbf{P}_{a}^{H} \mathfrak{U}_{k}(\mathbb{S}_{a}), \quad \mathcal{\Sigma}_{k}(\mathbb{S}_{a}) = \mathfrak{S}_{k}(\mathbb{S}_{a}) \mathbf{P}_{c},
\mathcal{V}_{k}(\mathbb{S}_{a}) = \mathbf{P}_{b} \mathfrak{V}_{k}(\mathbb{S}_{a}) \mathbf{P}_{c},$$
(39)

where $P_c \in \mathbb{R}^{(p+1)N_q \times (p+1)N_q}$ is the corresponding permutation matrix.

Compared to the original direct computation of the SVD of $\Delta \mathbb{Y}_{k,s}(\mathbb{S}_a)$, the computation complexity of the proposed algorithm becomes $\mathcal{O}(p(p+1)^2N_q)$ —two orders of magnitude lower than that of the original one with respect to N_q , the total number of effective frequencies.

The proposed DDRO-ILC method is summarized in Algorithm 1.

4. Experimental example

We illustrate and evaluate the DDRO-ILC technique by applying it to a multi-axis (3-axis) nanopositioning output tracking experiment. Two systems each of weak and strong cross-axis coupling, respectively, were considered.

Algorithm 1 The DDRO-ILC Algorithm

- 1: Quantify system noise level, ε_n , and the lower bound of system gain, \underline{h}_g .
- 2: Determine the threshold ϵ_Y , the effective frequency set \mathbb{S}_a , and the trackable desired output $\mathbf{Y}_d(\mathbb{S}_a)$.
- 3: Generate the initialization input, $u_{m,i}^{int}(t)$ for $i=1,\cdots,p$ (Eq. (15)) such that $\Psi(\omega_l)$ in Lemma 1 is nonsingular.
- 4: Apply $u_{m,i}^{int}(t)$ $(i=1,\cdots,p)$ to the system, respectively, and acquire $\boldsymbol{U}_{i}^{int}(\mathbb{S}_{a})$ and $\boldsymbol{Y}_{i}^{int}(\mathbb{S}_{a})$.
- 5: Generate $\mathbb{U}^{int}(\mathbb{S}_a)$ and $\mathbb{Y}^{int}(\mathbb{S}_a)$ from $\boldsymbol{U}_i^{int}(\mathbb{S}_a)$ and $\boldsymbol{Y}_i^{int}(\mathbb{S}_a)$ by Eq. (7), and form $\boldsymbol{U}_1(\mathbb{S}_a)$ by Eq. (6).
- 6: Generate the permutation matrices P_a , P_b and P_c in Eqs. (37), (39), (40), respectively.
- 7: **for** iteration k > 2 **do**
- 8: Apply $\boldsymbol{U}_{k-1}(\mathbb{S}_a)$ to the system and acquire $\boldsymbol{Y}_{k-1}(\mathbb{S}_a)$, $\Delta \mathbb{V}_{k-1,s}(\mathbb{S}_a)$, $\Delta \mathbb{Y}_{k-1,s}(\mathbb{S}_a)$ and $\boldsymbol{E}_{k-1}(\mathbb{S}_a)$.
- 9: Calculate the pseudoinverse of $\Delta \mathbb{Y}_{k-1,s}^{\dagger}(\mathbb{S}_a)$ by fSVD and generate $\Phi_{k-1}(\mathbb{S}_a)$ by choosing $\phi_{k-1}(\mathbb{S}_a)$ according to Corollary 1.
- 10: Determine $\boldsymbol{U}_{k}(\mathbb{S}_{a})$ using Eq. (6) from $\boldsymbol{U}_{k-1}(\mathbb{S}_{a})$, $\Delta \mathbb{U}_{k-1,s}(\mathbb{S}_{a})$, $\Delta \mathbb{Y}_{k-1,s}^{\dagger}(\mathbb{S}_{a})$, $\boldsymbol{\Phi}_{k-1}(\mathbb{S}_{a})$ and $\boldsymbol{E}_{k-1}(\mathbb{S}_{a})$
- 11: Set $k \leftarrow k+1$, repeat steps 8 to 10 until the error is within the bound of $\mathcal{H}(\varepsilon_n)$.
- 12: end for

4.1. Experimental setup

The *x*-*y*-*z* axes nanopositioning system of an AFM system (Dimension ICON, Bruker-Nano Inc.), composed by two piezoelectric actuators, was employed as the MIMO system to control. The system served well as a testbed for its wide application in nanopositioning control ranging from AFM imaging (Wu, Fang, Fan, Wang, & Liu, 2021), nanomanipulation (Li, Xi, Wang, & Liu, 2019), to nanomanufacturing (Loganathan & Bristow, 2014). All the control algorithms and inputs were generated in the MATLAB XPC-target environment (Mathworks Inc.) and applied to the AFM system via a DAQ system (NI-6259, National Instruments Inc.). The PID controller of the AFM system was bypassed when external control inputs were applied. The sampling rate was set at 40 kHz.

To evaluate the efficacy of the proposed technique in accounting of cross-axis coupling, a static-gain matrix C_w (see Fig. 1) was introduced to adjust the cross-axis coupling, i.e., the joint systems, $\hat{G}_p(s) = C_w G_p(s)$, was treated as the system to control, and in the implementation the control inputs were multiplied with the gain matrix C_w before they were sent out to drive the piezoelectric actuators. Based on the measured cross-axis dynamics coupling of the piezo actuators $G_p(s)$, the gain matrix C_w was set as

$$C_w = \begin{bmatrix} 1 & 0 & 0 \\ 0 & 1 & 0 \\ 0 & 0 & 1 \end{bmatrix}$$
, and $C_w = \begin{bmatrix} 1 & 0.8 & 0.6 \\ 0.7 & 1 & 0.8 \\ 0.8 & 0.4 & 1 \end{bmatrix}$,

for the weak and the strong coupling system, respectively. The measured frequency responses of these two cases are shown in Figs. 2. When the coupling was weak, the diagonal input–output (I/O) response dominated across the entire frequency range except for a small region around the resonant peaks (see Fig. 2 [a1-a3]), whereas the impact of the off-diagonal channel dynamics on each of three outputs was much more pronounced when the coupling was strong (see Fig. 2 [b1-b3]), making the tracking more challenging.

A tetrahedron pattern (see Fig. 3 [a]) was chosen as the desired trajectory at three different pattern-tracking rates, i.e., the rate of

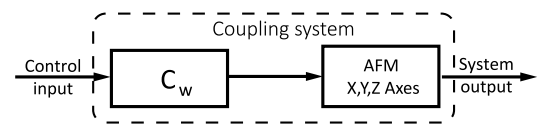


Fig. 1. Scheme of the 3D-axis nanopositoning system of an AFM with cross-axis coupling dynamics.

traversing the four triangular faces in order at 2, 20 and 40 Hz. For comparison, the pattern was also tracked by using the A-MAIIC and the DC-Gain methods (where the control input was generated by scaling the desired trajectory in each axis (see Fig. 3 [b]) with the inverse of the DC-Gain of the diagonal I/O response), respectively. Specifically, the A-MAIIC algorithm was based on the original multi-axis inversion-based iterative control (MAIIC) algorithm (Yan et al., 2012) by using the previous input-output data to adaptively update the diagonal inverse of the system in the iteration law,

$$\begin{split} \boldsymbol{u}_{k+1}(j\omega) &= \boldsymbol{u}_k(j\omega) + \zeta \hat{\boldsymbol{G}}_k^{-1}(j\omega)\boldsymbol{e}_k(j\omega), \ k \geq 1, \\ \text{where } \hat{\boldsymbol{G}}_k^{-1}(j\omega) &\in \mathbb{C}^{p \times p} \text{ and } \boldsymbol{\zeta} \in \mathbb{R}^{p \times p} \text{ were given as} \\ \hat{\boldsymbol{G}}_k^{-1}(j\omega) &= \operatorname{diag}\left(\left[\frac{y_{1,k}(j\omega)}{u_{1,k}(j\omega)} \ \cdots \ \frac{y_{p,k}(j\omega)}{u_{p,k}(j\omega)}\right]\right)_{p \times p}, \ \text{and} \\ \boldsymbol{\zeta} &= \operatorname{diag}\left(\left[\zeta_1 \ \cdots \ \zeta_p\right]\right)_{p \times p}, \end{split}$$

with ζ_i ($i=1,\ldots,p$) are the iteration coefficients. The DC-Gain method was employed to quantitatively illustrate the effects of both the vibrational dynamics and the cross-axis coupling on the output tracking. We also compare the computation time in the implementation of the DDRO-ILC via the SVD and the fSVD algorithm, respectively (see Fig. 3).

4.2. Experimental implementation

The DDRO-ILC method was implemented by following Algorithm 1. The optimal iterative gain matrix $oldsymbol{\phi}_k^* = oldsymbol{I}$ was chosen throughout the iterations and the threshold value for the disturbance level ϵ_Y was chosen at 1×10^{-4} , 2×10^{-4} and 5×10^{-4} for the 2 Hz, 20 Hz and 40 Hz patterns, respectively, and the number of corresponding effective frequencies to be tracked was chosen at 430, 400 and 390, respectively. As the rate of the trajectory increased, the effect of noise/disturbances became more pronounced, thus a larger threshold of ϵ_V was chosen, resulting in a smaller number of effective frequencies. The initialization input, $u_{m,i}^{int}(t)$, was designed by Eq. (15) with $\alpha_{m,i}=5.5,\ i=1,\ldots,\ p$, where $\alpha_{m,i}$ was designed according to the input amplitude constraint (-8.5 to 8.5 in our setup), and $\alpha = 5.5$ was chosen by Eq. (17). The A-MAIIC was implemented by choosing ζ = 1. During the experiment, the iterations were terminated when the relative two-norm error $E_2(\%)$ and the relative maximum tracking error $E_{max}(\%)$ could not be further reduced, where $E_2(\%)$ and $E_{max}(\%)$ were defined as

$$E_2(\%) = \frac{\|y_d(\cdot) - y(\cdot)\|_2}{\|y_d(\cdot)\|_2} \times 100\%,$$

$$E_{\text{max}}(\%) = \frac{\|y_d(\cdot) - y(\cdot)\|_{\infty}}{\|y_d(\cdot)\|_{\infty}} \times 100\%.$$

4.3. Results and discussion

The tracking results obtained via the DDRO-ILC technique are compared for the weak and the strong coupling system in Figs. 4 [a1-c1] and 5 [a1-c1], respectively. The tracking errors of the strong coupling system were shown in Fig. 6 [a1-c1]. For comparison, the tracking results obtained by the A-MAIIC and

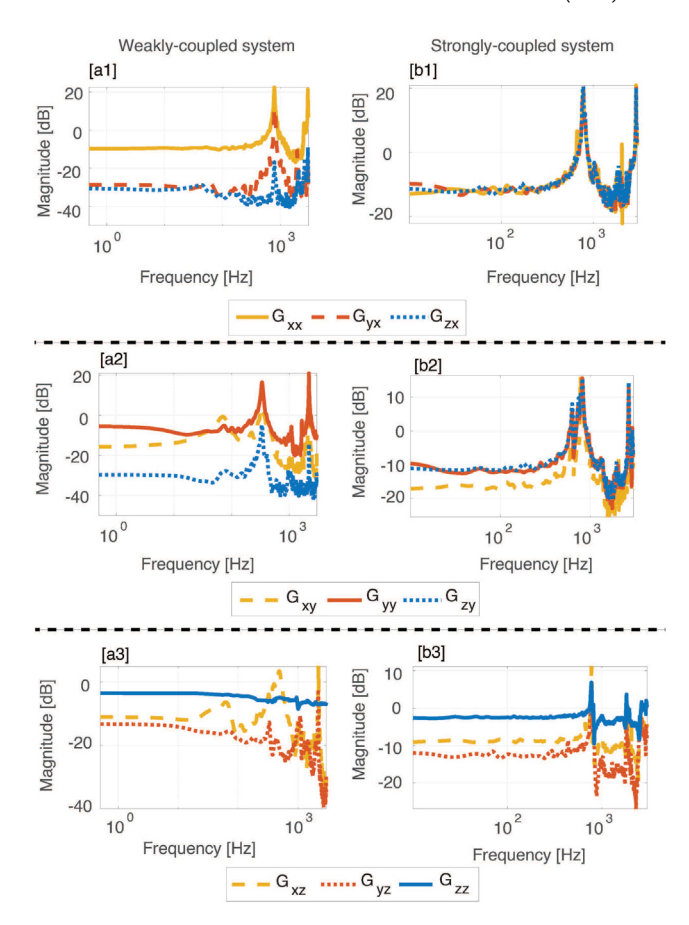


Fig. 2. Comparison of the frequency response of the x [a1, b1], y [a2, b2] and z [a3, b3] axis piezo actuator and the related coupling dynamics in the weaklyand the strongly- coupled system, respectively.

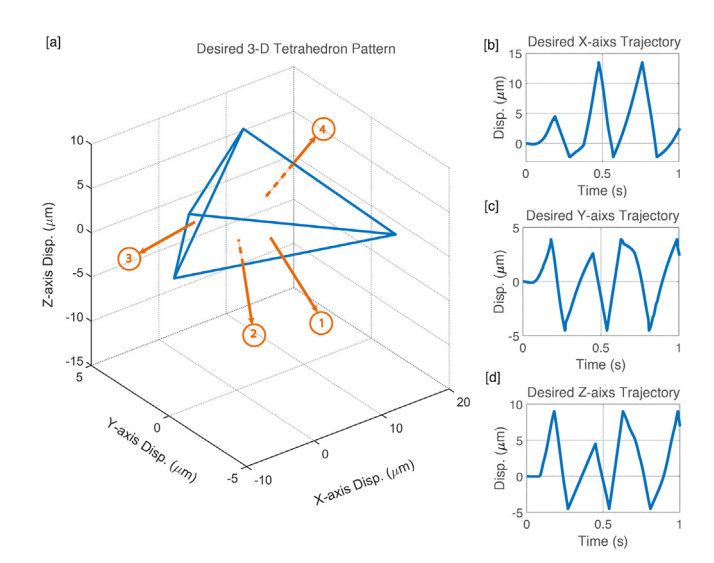


Fig. 3. The desired trajectory of the 3-D tetrahedron pattern [a], and the corresponding desired trajectory in x, y, and z axes [b-d], respectively.

the DC-Gain methods are shown in Figs. 4 [a2-c2] and 5 [a2-c2], respectively. The corresponding tracking errors of the strong coupling system are shown in Figs. 6 [a2-c2]. The convergence processes are shown in Fig. 7. The average computation time in each iteration of the DDRO-ILC algorithm by using the SVD and fSVD algorithm, respectively, are shown in Fig. 8 for the tracking in the strong coupling case.

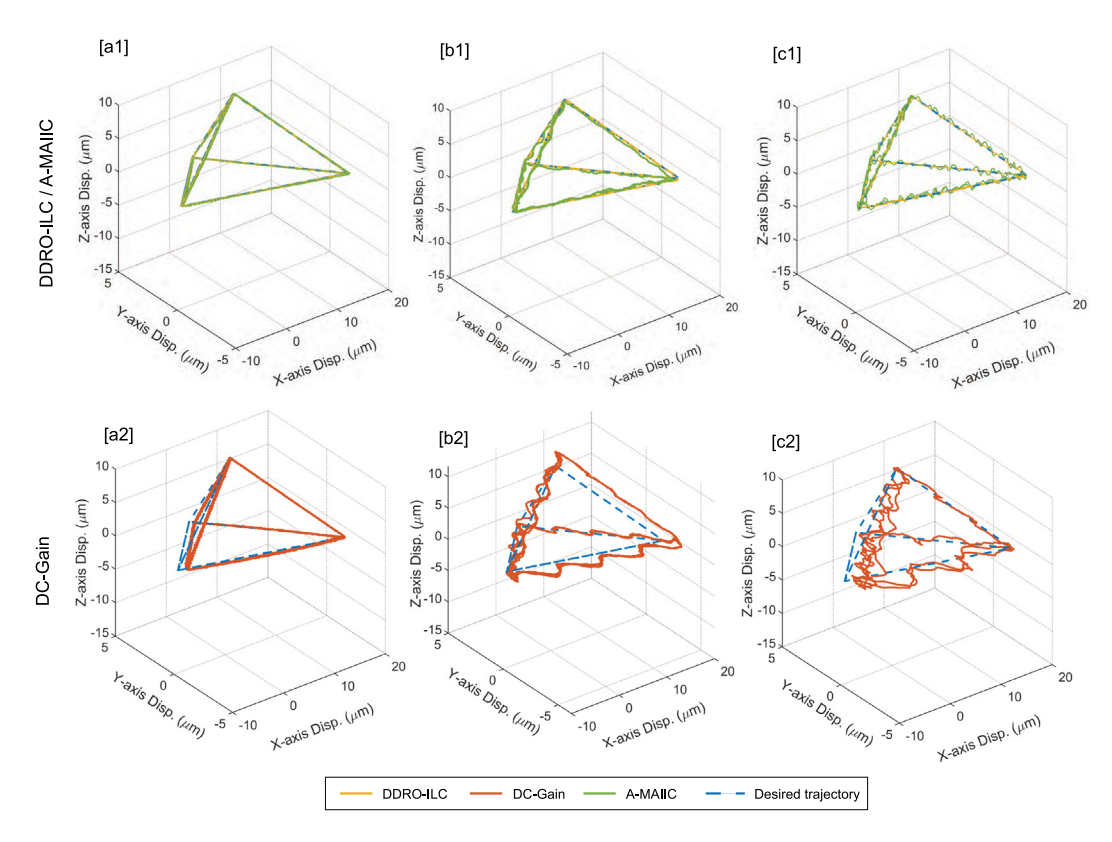


Fig. 4. Comparison of the tracking of the tetrahedron pattern on the weakly-coupled system obtained by using the DDRO-ILC technique with those by using the A-MAIIC and DC-Gain techniques at 2 Hz [a1-a2], 20 Hz [b1-b2] and 40 Hz [c1-c2], respectively.

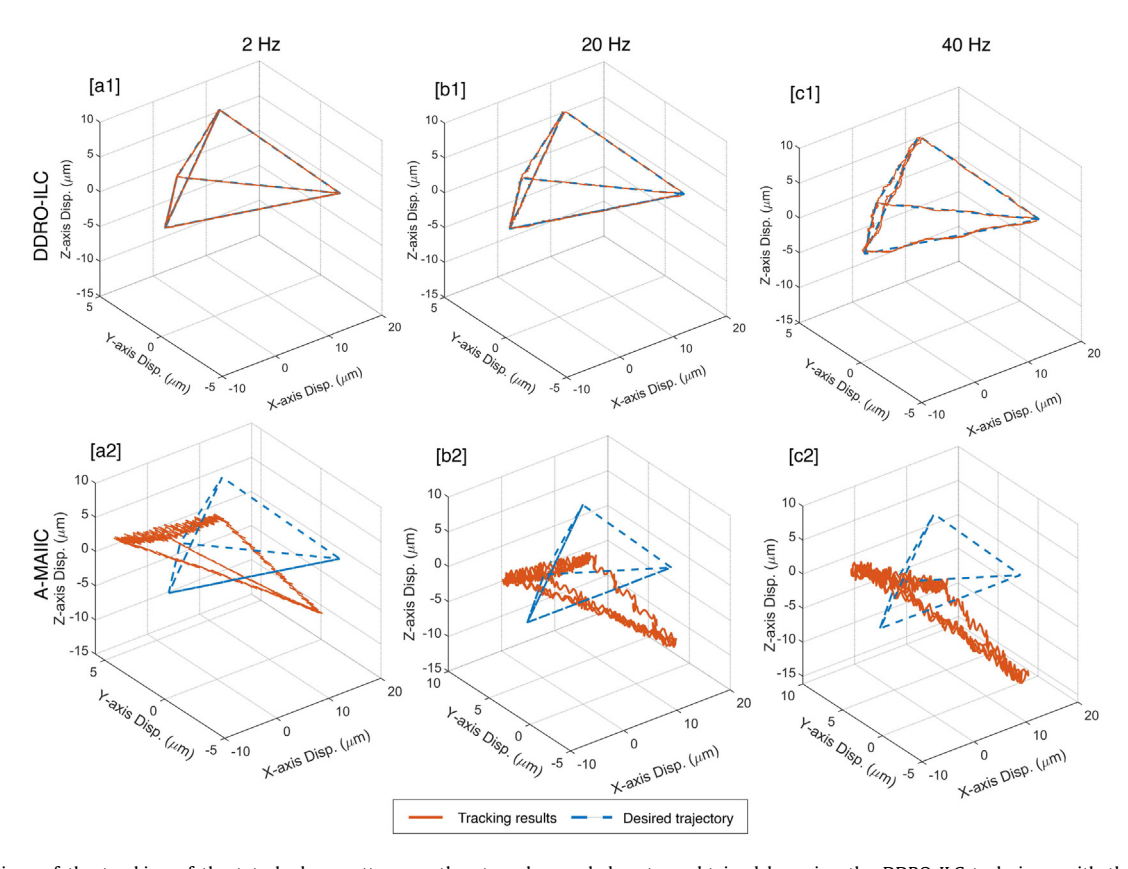


Fig. 5. Comparison of the tracking of the tetrahedron pattern on the strongly-coupled system obtained by using the DDRO-ILC technique with those obtained by using the A-MAIIC technique at 2 Hz [a1-a2], 20 Hz [b1-b2] and 40 Hz [c1-c2], respectively..

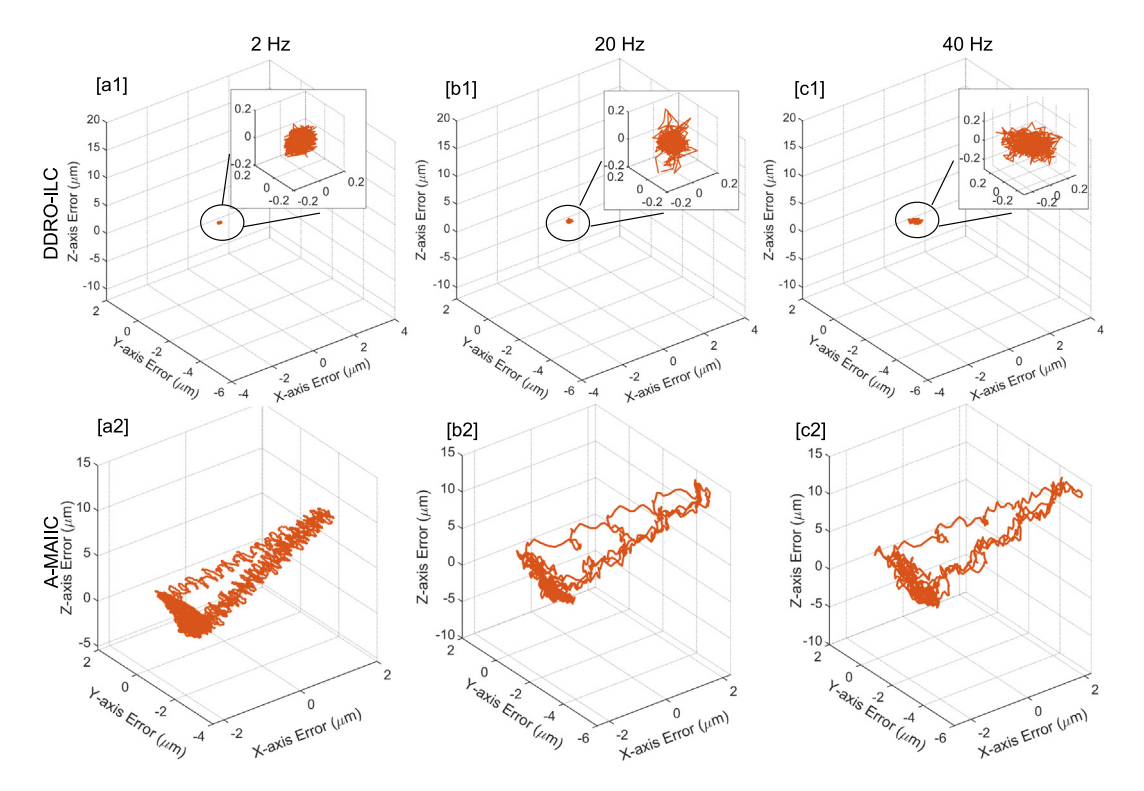


Fig. 6. Comparison of the tracking error on the strongly-coupled system obtained by using the DDRO-ILC technique with those obtained by using the A-MAIIC technique at 2 Hz [a1-a2], 20 Hz [b1-b2] and 40 Hz [c1-c2], respectively..

4.3.1. Weakly-coupled system case

The experimental results demonstrated that the proposed DDRO-ILC method improved the tracking performance over the previous A-MAIIC method. As shown in Figs. 4 [a2], at the low rate of 2 Hz, the effect of the dynamics and the coupling effects were relatively small. Both the DDRO-ILC and the A-MAIIC technique can achieve precision tracking (see Figs. 4 [a1, a2]), and the tracking performance of the proposed DDRO-ILC method was better than that of the A-MAIIC method. The 2-norm tracking error of the proposed DDRO-ILC method was about 10 times smaller than those of the A-MAIIC method, reduced from 4.83%, 4.49% and 4.50% to 0.37%, 0.59% and 0.38% for the x, y and zaxis tracking, respectively. As the pattern rate was increased to 20 Hz (see Figs. 4 [b1, b2]), the dynamics effect became more pronounced (see the DC-Gain tracking results in Figs. 4 [b2]), resulting in large tracking errors. However, by using the proposed DDRO-ILC technique, the tracking error of the A-MAIIC technique was substantially reduced by over 3 and 4 times in $E_2(\%)$ and $E_{\text{max}}(\%)$, respectively, clearly showing an improvement in robustness. This enhancement stemmed from the account of the system dynamics and the cross-axis coupling through the data-driven system inverse employed in the proposed DDRO-ILC technique, i.e., the cross-coupling effect was directly compensated for by inverting the whole system dynamics via pseudoinverse (see Eq. (10)), whereas it was treated as disturbances in the A-MAIIC technique. Such an improvement was further demonstrated in Figs. 4 [c1-c2] for tracking the pattern at higher rate of 40 Hz, where both the cross-coupling and the dynamics effect became more pronounced (see Figs. 4 [c2]). With both the $E_2(\%)$ and the $E_{\text{max}}(\%)$ maintained below 4%, precision tracking was still attained by using the DDRO-ILC technique. Thus, the proposed DDRO-ILC technique was effective for output tracking of MIMO systems.

4.3.2. Strongly-coupled system case

The efficacy of the proposed approach was more evidently demonstrated in the strongly-coupled case, where the crosscoupling effect dominated the outputs of the x and the y axes (see Fig. 2 [b1-b3]). Outstanding performance and precision tracking were still achieved by using the proposed DDRO-ILC technique (see Figs. 5 [a1-c1] and 6 [a1-c1]). For example, at the low rate of 2 Hz pattern rate, both the relative $E_2(\%)$ and the relative $E_{\text{max}}(\%)$ were less than 1% and 2%, respectively. Even in the tracking at 40 Hz pattern rate where the effects of both the dynamics and cross-axis coupling became more pronounced, the DDRO-ILC technique still preserved precision tracking, with the $E_2(\%)$ and the $E_{\text{max}}(\%)$ less than 3% and 4%, respectively. In contrast, as the Assumption of the diagonal-dynamics being dominant vanished, the tracking results of the A-MAIIC approach deteriorated (see Figs. 5 [a2-c2] and 6 [a2-c2]). This precision tracking for a MIMO system of strong cross coupling was achieved without modeling the system dynamics a priori-such a modeling process itself can be time consuming and complicated for strongly-coupled systems. Moreover, the variations of the system dynamics were automatically accounted for via the input-output data during the iterations. Also, as shown in Fig. 7, the DDRO-ILC algorithm converged rapidly and reached practical convergence in three iterations for both the weakly-coupled and the strong-coupled systems in high speed tracking. Thus, the proposed DDRO-ILC technique was efficient and effective for output tracking of strong-coupling MIMO systems.

Finally, the experimental results also showed that the computation efficiency was improved by using the proposed fSVD algorithm. As shown in Fig. 8, the computation time was reduced by over 19.7%, 19.2% and 18.7% for the tracking of pattern rate at 2 Hz, 20 Hz and 40 Hz, respectively. The decrease of the computation reduction as the pattern rate increased was due to the reduction of the number of effective frequencies (with the reduction of the SNR at higher frequency), as the computation

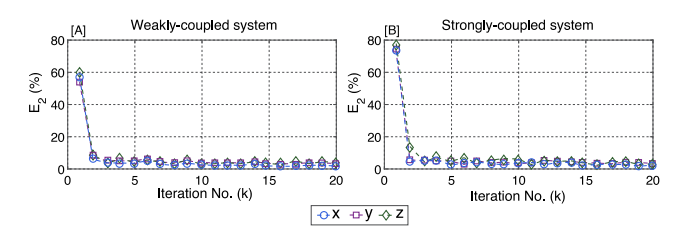


Fig. 7. The relative 2-norm overall error in the 40 Hz tracking in 20 iterations for the weakly-coupled [A] and the strongly-coupled [B] system, respectively, obtained when using the DDRO-ILC technique.

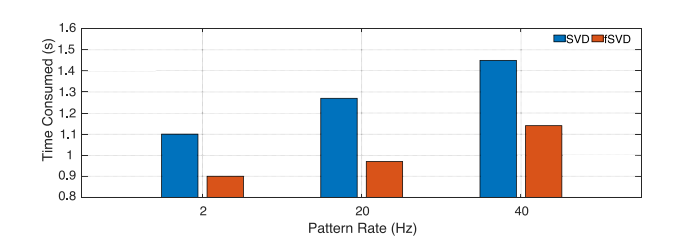


Fig. 8. Comparison of the average computation time during each iteration when using the the SVD or the fSVD algorithm in the implementation of the DDRO-LIC technique to track the pattern at the rate of 2 Hz, 20 Hz and 40 Hz, respectively, on the strongly-coupled system.

complexity is bounded as $\mathcal{O}(p(p+1)^2N_q^3)$ and $\mathcal{O}(p(p+1)^2N_q)$ for SVD and fSVD algorithm, respectively (see Section 3.5). Thus, the computation efficiency becomes more beneficial when tracking trajectories of richer spectrum.

5. Conclusion

A data-driven robust optimal iterative learning control (DDRO-ILC) approach for output tracking of MIMO linear systems was proposed. The input-output data measured in the previous iteration were utilized to approximate the system inverse and update the control input. It was shown that the convergence of the output tracking was guaranteed in the presence of crossaxis coupling dynamics and random output disturbance, and the iteration control gain can be optimized to minimize the residual tracking error and maximize the convergence rate. An algorithm to accelerate the input calculation via singular value decomposition was also proposed. Experimental implementation on output tracking of a 3-axis nanopositioning system demonstrated that the proposed DDRO-ILC technique had enhanced both the robustness and the tracking performance over the previous A-MAIIC method. For future work, the technique can be extended to account for more complicated dynamics and in more complicated tracking scenarios, including static nonlinearity in Hammerstein systems, MIMO nonlinear dynamic systems, and tracking under drift and time-delay effects.

Appendix A. Proof of Lemma 1

Proof. We proceed by constructing a matrix $\mathbb{P}^{int}(\mathbb{S}_a) \in \mathbb{C}^{pN_q \times pN_q}$

$$\mathbb{P}^{int}(\mathbb{S}_a) = \boldsymbol{\Psi}(\omega_1) \oplus \boldsymbol{\Psi}(\omega_2) \cdots \oplus \boldsymbol{\Psi}(\omega_{N_a}),$$

such that $\mathbb{P}^{int}(\mathbb{S}_a)$ is similar to $\mathbb{U}^{int}(\mathbb{S}_a)$. This can be verified as by Eq. (7),(13),(14), $\mathbb{U}^{int}(\mathbb{S}_a)$ can be represented by $\Gamma_{i,i}(\mathbb{S}_a)$ as

$$\mathbb{U}^{int}(\mathbb{S}_a) = \begin{bmatrix} \boldsymbol{\Gamma}_{1,1}(\mathbb{S}_a) & \cdots & \boldsymbol{\Gamma}_{1,p}(\mathbb{S}_a) \\ \vdots & \ddots & \vdots \\ \boldsymbol{\Gamma}_{p,1}(\mathbb{S}_a) & \cdots & \boldsymbol{\Gamma}_{p,p}(\mathbb{S}_a) \end{bmatrix}_{pN_a \times pN_a},$$

where $F_{j,i}(\mathbb{S}_a)$ is as given in Eq. (14). Then, it can be verified that by matrix permutation (Davis, 2006) that there exists a matrix $\mathbb{B}_{p,N_q} \in \mathbb{R}^{pN_q \times pN_q}$, such that

$$\mathbb{P}^{int}(\mathbb{S}_a) = \mathbb{B}_{p,N_q} \mathbb{U}^{int}(\mathbb{S}_a) \mathbb{B}_{p,N_q}^T, \tag{A.1}$$

with

$$\mathbb{B}_{p,N_q} = \sum_{i=1}^p \sum_{j=1}^{N_q} (e_i^{(p)} \otimes e_j^{(N_q)}) (e_j^{(N_q)} \otimes e_i^{(p)})^T, \tag{A.2}$$

where $e_i^{(p)}$ denotes the ith canonical basis vector of \mathbb{R}^p (the ith column of the size m identity matrix), and \otimes is the Kronecker product (Horn & Johnson, 2012). As the permutation matrix is orthogonal (Horn & Johnson, 2012), by Eq. (A.1), $\mathbb{P}^{int}(\mathbb{S}_a)$ is similar to $\mathbb{U}^{int}(\mathbb{S}_a)$.

Thus, as $\mathbb{P}^{int}(\mathbb{S}_a)$ is block diagonal and similar to $\mathbb{U}^{int}(\mathbb{S}_a)$, nonsingularity of $\Psi(\omega_l)$ implies that both $\mathbb{P}^{int}(\mathbb{S}_a)$ and $\mathbb{U}^{int}(\mathbb{S}_a)$ are nonsingular.

Reversely, if $\mathbb{U}^{int}(\mathbb{S}_a)$ is nonsingular, $\mathbb{P}^{int}(\mathbb{S}_a)$ being similar to $\mathbb{U}^{int}(\mathbb{S}_a)$ implies that $\mathbb{P}^{int}(\mathbb{S}_a)$ is also nonsingular, so is each block diagonal submatrix of $\mathbb{P}^{int}(\mathbb{S}_a)$, $\Psi(\omega_l)$. This completes the proof. \square

Appendix B. Proof of Corollary 1

Proof. First by Theorem 1, $\mathbb{A} = \{k | \|\mathbf{E}_k(\mathbb{S}_a)\|_2 \le \mathcal{H}(\varepsilon_n)\} \ne \emptyset$, and, by Eq. (35), the propagation of $\|\mathbf{E}_k(\mathbb{S}_a)\|_2$ can be bounded by

$$\|\mathbf{E}_{k}(\mathbb{S}_{q})\|_{2} - \|\mathbf{E}_{k-1}(\mathbb{S}_{q})\|_{2} < (\overline{\eta} - 1)\|\mathbf{E}_{k-1}(\mathbb{S}_{q})\|_{2} + 2\varepsilon_{n}.$$
 (B.1)

Also, by Definition 2,

$$\|\mathbf{E}_{k}(\mathbb{S}_{a})\|_{2} > \mathcal{H}(\varepsilon_{n}) = \frac{2\varepsilon_{n}}{1 - \overline{\eta}}, \quad \text{for } \forall k < k^{*}(\mathcal{H}(\varepsilon_{n})),$$
 (B.2)

where k^* is as in Definition 2. Thus, the proof is completed by combining Eq. (B.2) with Eq. (B.1)

$$\|\mathbf{E}_k(\mathbb{S}_a)\|_2 - \|\mathbf{E}_{k-1}(\mathbb{S}_a)\|_2 < (\overline{\eta} - 1)\frac{2\varepsilon_n}{1 - \overline{n}} + 2\varepsilon = 0,$$

for $\forall k < k^*(\mathcal{H}(\varepsilon_n))$. \square

References

Aarnoudse, Leontine, & Oomen, Tom (2020). Model-free learning for massive MIMO systems: Stochastic approximation adjoint iterative learning control. *IEEE Control Systems Letters*, 5(6), 1946–1951.

Anderson, Edward, Bai, Zhaojun, Bischof, Christian, Blackford, L Susan, Demmel, James, Dongarra, Jack, et al. (1999). LAPACK users' guide. SIAM.

Armstrong, Ashley A., & Alleyne, Andrew G. (2021). A multi-input single-output iterative learning control for improved material placement in extrusion-based additive manufacturing. *Control Engineering Practice*, 111, Article 104783

Bolder, Joost, Kleinendorst, Stephan, & Oomen, Tom (2018). Data-driven multivariable ILC: enhanced performance by eliminating L and Q filters. *International Journal of Robust and Nonlinear Control*, 28(12), 3728–3751.

Bristow, D. A., Tharayil, M., & Alleyne, A. G. (2006). A survey of iterative learning control. *IEEE Control Systems Magazine*, 26(3), 96–114.

Brunton, Steven L., & Kutz, J. Nathan (2022). Data-driven science and engineering:

Machine learning, dynamical systems, and control. Cambridge University Press. Chen, Wenjie, & Tomizuka, Masayoshi (2013). Dual-stage iterative learning control for MIMO mismatched system with application to robots with joint elasticity. IEEE Transactions on Control Systems Technology, 22(4), 1350–1361.

Davis, Timothy A. (2006). Direct methods for sparse linear systems. SIAM.

Devasia, Santosh, & Paden, B. (1998). Stable inversion for nonlinear nonminimum-phase time-varying systems. *IEEE Transactions on Automatic Control*, 43(2), 283–288.

Dirkx, Nic, van de Wijdeven, Jeroen, & Oomen, Tom (2020). Frequency response function identification for multivariable motion control: Optimal experiment design with element-wise constraints. *Mechatronics*, 71, Article 102440.

Hao, Xiaohong, Zhang, Lei, & Li, Hengjie (2008). A new PD type iterative learning control in active control for vibration. In 2008 7th world congress on intelligent control and automation (pp. 922–926). IEEE.

Horn, Roger A., & Johnson, Charles R. (2012). Matrix analysis. Cambridge University Press.

Hungerford, Thomas W. (2012). Abstract algebra: An introduction. Cengage Learning.

Khalil, H. K. (2011). Nonlinear systems. Prentice-Hall.

Li, Mi, Xi, Ning, Wang, Yuechao, & Liu, Lianqing (2019). Advances in atomic force microscopy for single-cell analysis. *Nano Research*, 12(4), 703–718.

Lin, Pei-Yu, Lee, Jung-San, & Chang, Chin-Chen (2009). Distortion-free secret image sharing mechanism using modulus operator. *Pattern Recognition*, 42(5), 886–895.

Loganathan, Muthukumaran, & Bristow, Douglas A. (2014). Bi-harmonic cantilever design for improved measurement sensitivity in tapping-mode atomic force microscopy. *Review of Scientific Instruments*, 85(4), Article 043703.

Mandra, Slawomir, Galkowski, Krzysztof, Rauh, Andreas, Aschemann, Harald, & Rogers, Eric (2020). Iterative learning control for a class of multivariable distributed systems with experimental validation. *IEEE Transactions on Control Systems Technology*, 29(3), 949–960.

Oppenheimer, Michael W., Doman, David B., & Bolender, Michael A. (2006). Control allocation for over-actuated systems. In 2006 14th mediterranean conference on control and automation (pp. 1–6).

Schkoda, Ryan (2007). Dynamic inversion of underactuated systems via squaring transformation matrix.

Skogestad, Sigurd, & Postlethwaite, Ian (2007). Multivariable feedback control: analysis and design: vol. 2, Citeseer.

Wang, Zhihua, & Zou, Qingze (2023). Simultaneous hysteresis-dynamics compensation in high-speed, large-range trajectory tracking: A data-driven iterative control. *International Journal of Robust and Nonlinear Control*, 33(1), 489–506.

Wu, Yinan, Fang, Yongchun, Fan, Zhi, Wang, Chao, & Liu, Cunhuan (2021).
An automated vertical drift correction algorithm for AFM images based on morphology prediction. *Micron*, 140, Article 102950.

Yan, Leon Liangwu, Banka, Nathan, Owan, Parker, Piaskowy, Walter Tony, Garbini, Joseph L, & Devasia, Santosh (2021). MIMO ILC using complex-kernel regression and application to precision SEA robots. *Automatica*, 127, Article 109550

Yan, Yan, Wang, Haiming, & Zou, Qingze (2012). A decoupled inversion-based iterative control approach to multi-axis precision positioning: 3D nanopositioning example. *Automatica*, 48(1), 167–176.

Yu, Xian, Hou, Zhongsheng, Polycarpou, Marios M., & Duan, Li (2020). Datadriven iterative learning control for nonlinear discrete-time MIMO systems. IEEE Transactions on Neural Networks and Learning Systems, 32(3), 1136–1148.

Zhang, Zezhou, & Zou, Qingze (2023). Data-driven robust optimal iterative learning control of linear systems with strong cross-axis coupling. In 2023 American control conference. IEEE.



Zezhou Zhang received the B.S. degree and M.S. degree in automation from the University of Electronic Science and Technology of China, Chengdu, China, in 2016 and 2019. He is currently pursuing the Ph.D. degree in mechanical engineering at the Department of Mechanical and Aerospace Engineering, Rutgers University, Piscataway, NJ, USA. His research interests are data-driven modeling and control with applications in precision tracking and motion control.



Qingze Zou received his Ph.D. in mechanical engineering from the University of Washington, Seattle, WA, USA in 2003, MS. in mechanical engineering from Singhua University, Beijing, China in 1997, and BS. in Automatic Control from the University of Electronic Science and Technology of China, Chengdu, China in 1994. He is a Professor of mechanical and aerospace engineering at Rutgers, the State University of New Jersey, Piscataway, NJ, USA. Previously he had taught at the Iowa State University, USA. His research interests include learning-based precision tracking and motion

control, control of high-speed scanning probe microscopy, nanoscale acoustic noise control, stomata dynamics modeling and measurement, and robotic remanufacturing. Dr. Zou received the NSF CAREER Award in 2009, and the O. Hugo Schuck Best Paper Award from the American Automatic Control Council in 2010. He was an Associate Editor of ASME Journal of Dynamic Systems, Measurement and Control, IFAC-Control Engineering Practice, and IFAC-Mechatronics, and a Technical Editor of IEEE/ASME Transactions on Mechatronics. Currently he is a Senior Editor of IEEE/ASME Transactions on Mechatronics, and the lead Guest Editor of the 4th and 5th focused section on the TMECH/AIM emerging topics. He is a Fellow of ASME.